

Neuron

Input-Timing-Dependent Plasticity in the Hippocampal CA2 Region and Its Potential Role in Social Memory

Highlights

- CA2 shows input-timing-dependent plasticity after pairing of its EC and SC inputs
- CA2 ITDP results from long-term depression of PV⁺ IN feedforward inhibition
- CA2 ITDP relies on activation of δ -opioid receptors expressed in PV⁺ INs
- CA2 ITDP potentiates net SC \rightarrow CA2 excitation and is associated with social memory

Authors

Felix Leroy, David H. Brann, Torcato Meira, Steven A. Siegelbaum

Correspondence

felxfel@aol.com (F.L.),
sas8@columbia.edu (S.A.S.)

In Brief

Paired activation of cortical and hippocampal inputs induces input-timing-dependent plasticity (ITDP) in CA1 neurons, enhancing contextual memory specificity. Here, Leroy et al. report that a distinct form of ITDP is associated with social memory storage in CA2 neurons.



Input-Timing-Dependent Plasticity in the Hippocampal CA2 Region and Its Potential Role in Social Memory

Felix Leroy,^{1,*} David H. Brann,¹ Torcato Meira,^{1,2,3} and Steven A. Siegelbaum^{1,4,*}

¹Department of Neuroscience, Kavli Institute of Brain Science, Columbia University Medical Center, 1051 Riverside Drive, New York, NY, USA

²Life and Health Sciences Research Institute (ICVS), School of Medicine, University of Minho, Braga, Portugal

³ICVS/3B's, PT Government Associate Laboratory, Braga/Guimarães, Portugal

⁴Lead Contact

*Correspondence: felxfel@aol.com (F.L.), sas8@columbia.edu (S.A.S.)

<http://dx.doi.org/10.1016/j.neuron.2017.07.036>

SUMMARY

Input-timing-dependent plasticity (ITDP) is a circuit-based synaptic learning rule by which paired activation of entorhinal cortical (EC) and Schaffer collateral (SC) inputs to hippocampal CA1 pyramidal neurons (PNs) produces a long-term enhancement of SC excitation. We now find that paired stimulation of EC and SC inputs also induces ITDP of SC excitation of CA2 PNs. However, whereas CA1 ITDP results from long-term depression of feedforward inhibition (iLTD) as a result of activation of CB1 endocannabinoid receptors on cholecystokinin-expressing interneurons, CA2 ITDP results from iLTD through activation of δ -opioid receptors on parvalbumin-expressing interneurons. Furthermore, whereas CA1 ITDP has been previously linked to enhanced specificity of contextual memory, we find that CA2 ITDP is associated with enhanced social memory. Thus, ITDP may provide a general synaptic learning rule for distinct forms of hippocampal-dependent memory mediated by distinct hippocampal regions.

INTRODUCTION

Most studies of the role of long-term synaptic plasticity in learning and memory have focused on Hebbian plasticity, in which activity in a given excitatory pathway leads to homosynaptic changes in the activated synapses (Alger and Teyler, 1976; Bliss and Lomo, 1973). The induction of such forms of plasticity often requires strong, high-frequency tetanic stimulation, as in the induction of long-term potentiation of excitatory transmission at the Schaffer collateral (SC) synapses onto hippocampal CA1 pyramidal neurons (PNs) in response to one or more bursts of 100 Hz tetanic stimulation. However, such prolonged high-frequency activation may not occur under physiological conditions, where hippocampal neuron firing tends to be sparse (Kowalski et al., 2016).

Heterosynaptic forms of plasticity, where activation of one input modulates the strength of a second input, provide a distinct mechanism for altering the strength of synaptic transmission. These forms of plasticity have been described in various parts of the brain, including cerebellum (Ito, 2001; Safo and Regehr, 2008) and amygdala (Cho et al., 2011), with mechanisms that are often tuned to the particular properties of the given circuit. However, the importance of heterosynaptic forms of plasticity in the hippocampus has been less widely investigated.

Our laboratory described a circuit-based form of heterosynaptic plasticity, termed input-timing-dependent plasticity (ITDP), in which low-frequency, paired activation of the long-range, direct entorhinal cortex (EC) inputs to CA1 PNs precisely 20 ms prior to activation of the local SC inputs from hippocampal CA3 neurons produces a long-term enhancement of SC-evoked excitation of CA1 (Basu et al., 2013; Dudman et al., 2007). The increase in SC-evoked synaptic depolarization of CA1 results largely from the long-term depression of feedforward inhibition (iLTD) mediated by cholecystokinin-expressing (CCK⁺) interneurons (INs) through the activation of endocannabinoid CB1 receptors (Basu et al., 2013), with a smaller component of ITDP caused by potentiation of SC excitatory synaptic transmission (eLTP). Unlike conventional LTP, ITDP can be induced by weak sub-threshold paired stimuli at a low (1 Hz) frequency, similar to that observed during *in vivo* recordings (Csicsvari et al., 1999; Frank et al., 2001). Of particular interest, the ITDP pairing interval matches the delay line architecture inherent in the cortico-hippocampal circuit, in which information from EC arrives at CA1 through the direct path, approximately 15–20 ms prior to transmission through the indirect trisynaptic pathway: (EC → dentate gyrus [DG] → CA3 → CA1; Yeckel and Berger, 1990). Thus, ITDP was proposed to provide a mechanism to assess the salience of mnemonic information relayed to a given CA1 PN through its local CA3 inputs based on its temporal relation to sensory contextual information conveyed by its long-range, direct EC inputs. Indeed, a recent study suggests that CA1 ITDP may serve to enhance the specificity of contextual fear memory and the strength of object recognition memory (Basu et al., 2016).

One question raised by these previous findings is whether ITDP is specific to CA1 or whether it might serve as a more widespread synaptic learning rule as other hippocampal regions receive both long-range and local excitatory inputs. Here, we

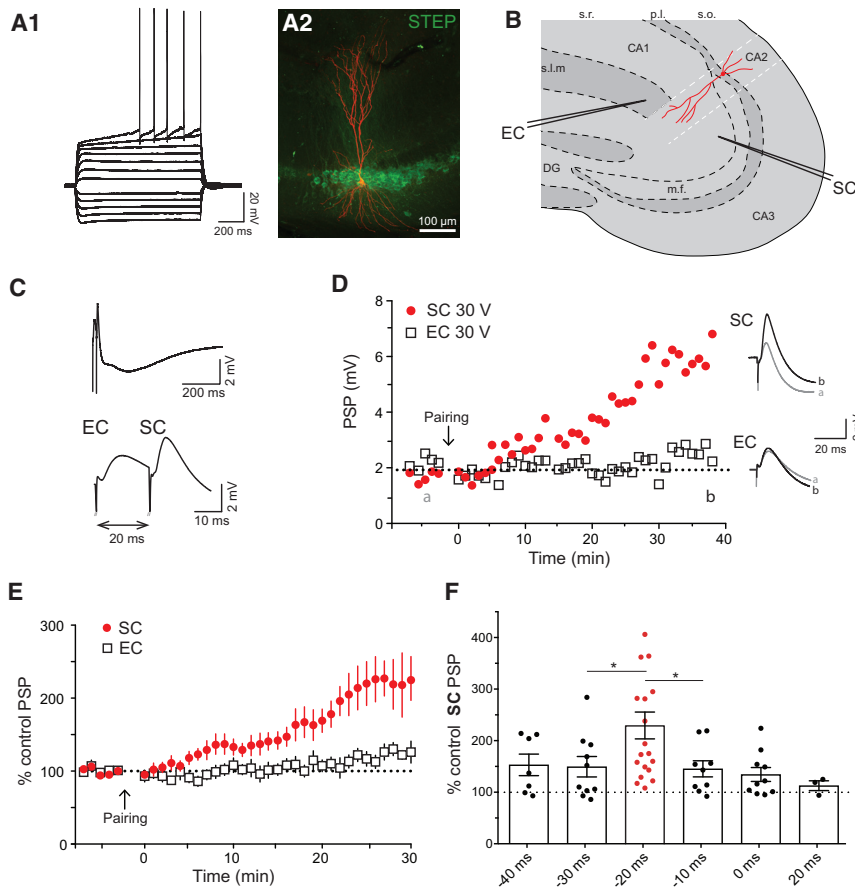


Figure 1. CA2 PNs Display ITDP

(A) Whole-cell current-clamp recording showing injection of 25 pA current steps (A1). Streptavidin (red) and CA2 marker STEP (green) immunohistochemistry of the biocytin-filled PN (A2).

(B) Drawing of the localization of the stimulating electrodes in the hippocampal slice.

(C) Current-clamp response during a single EC+SC pairing in the ITDP induction protocol (repeated 90 times at 1 Hz). The bottom trace is an enlargement of the upper one.

(D) Time course of the EC and SC PSPs amplitudes obtained in current clamp following ITDP induction (left). The right displays the SC and EC PSP before (gray) and after (black) ITDP. Data from (A) to (C) (and from Figure S1) are from the same CA2 PN.

(E) Time course of the average normalized PSP amplitudes obtained in whole-cell current clamp following ITDP induction.

(F) Normalized SC PSP amplitudes following ITDP induction using different intervals between the EC and SC stimulation (-20 ms indicates EC followed by the SC 20 ms later). Data are represented as mean \pm SEM. See also Figure S1.

have focused on plasticity mechanisms in the hippocampal CA2 region, which has recently shown to be important for social memory, the ability of an animal to recognize and remember a conspecific (Hitti and Siegelbaum, 2014; Stevenson and Caldwell, 2014). As CA2 PNs also receive direct, long-range inputs from EC and local inputs conveyed by the trisynaptic path (EC \rightarrow DG \rightarrow CA3 \rightarrow CA2), we investigated whether ITDP can also be induced at CA2 PN synapses and whether plasticity mechanisms related to ITDP may be associated with social memory.

RESULTS

Electrical Pairing of EC and SC CA2 Inputs at a 20 ms Interval Induces ITDP

We first examined whether paired electrical stimulation of the EC and SC inputs was able to induce ITDP of either EC or SC excitation of CA2 PNs. We recorded from CA2 PNs in dorsal hippocampal slices, confirming neuronal identity by electrophysiological (Figure 1A1), morphological (Figures 1A2 and 3F), and molecular properties (Figures 1A2, 4E3, and 6E3; see STAR Methods). One stimulating electrode was placed in the *stratum lacunosum-moleculare* (SLM) of CA1c, near the hippocampal fissure to activate the direct EC inputs and a second placed in the *stratum radiatum* (SR) of CA3 near the CA2 border to activate SC inputs (Figure 1B1) as described (Chevalleyre and Siegelbaum, 2010). Stimulating voltage intensity was adjusted (range from

5 to 50 V) to elicit postsynaptic potentials (PSPs) with an ~ 3 mV peak amplitude (Figure 1D). Following 5 min of stable baseline recording, we applied an ITDP induction protocol in CA2 that is maximally effective in CA1, consisting of 90 pairs of EC+SC stimulating pulses at a frequency of 1 Hz, at a -20 ms pairing interval (EC stimulated

20 ms before SC stimulation; Dudman et al., 2007). The paired stimuli produced a small depolarization that never reached threshold for triggering a postsynaptic CA2 action potential.

Several minutes after applying the ITDP pairing protocol, the SC-evoked PSP started to increase in amplitude, reaching a plateau level of potentiation after 30 min of $229\% \pm 26\%$ relative to baseline ($n = 19$ neurons; Wilcoxon test, $p < 0.0001$, Figures 1C–1E). This is similar to the magnitude of ITDP in CA1 (PSP increased to $\sim 250\%$ of baseline; Basu et al., 2013; Dudman et al., 2007). In contrast to the lack of ITDP in the EC inputs to CA1 (Basu et al., 2013; Dudman et al., 2007), we observed a significant, but small, increase in the EC-evoked PSP to $138\% \pm 13\%$ of baseline ($n = 17$; Wilcoxon test, $p = 0.002$ compared to baseline, Figures 1C–1E). The large increase in the SC PSP was observed throughout the entire range of voltage stimulation intensity, with the EC PSP showing a more modest increase (Figure S1).

In CA1, ITDP is finely tuned to the -20 ms pairing interval (EC before SC), with little or no potentiation at other pairing intervals (Basu and Siegelbaum, 2015; Dudman et al., 2007). We thus tested the interval dependence of ITDP induction in CA2 using a range of pairing delays (Figure 1F). As in CA1, the extent of CA2 ITDP was greatest at the -20 ms interval. When we reversed the pairing order, stimulating SC inputs 20 ms before EC inputs, we failed to significantly alter the SC PSP ($108\% \pm 12\%$, $n = 5$; Wilcoxon test, $p = 0.3$ compared to baseline), similar

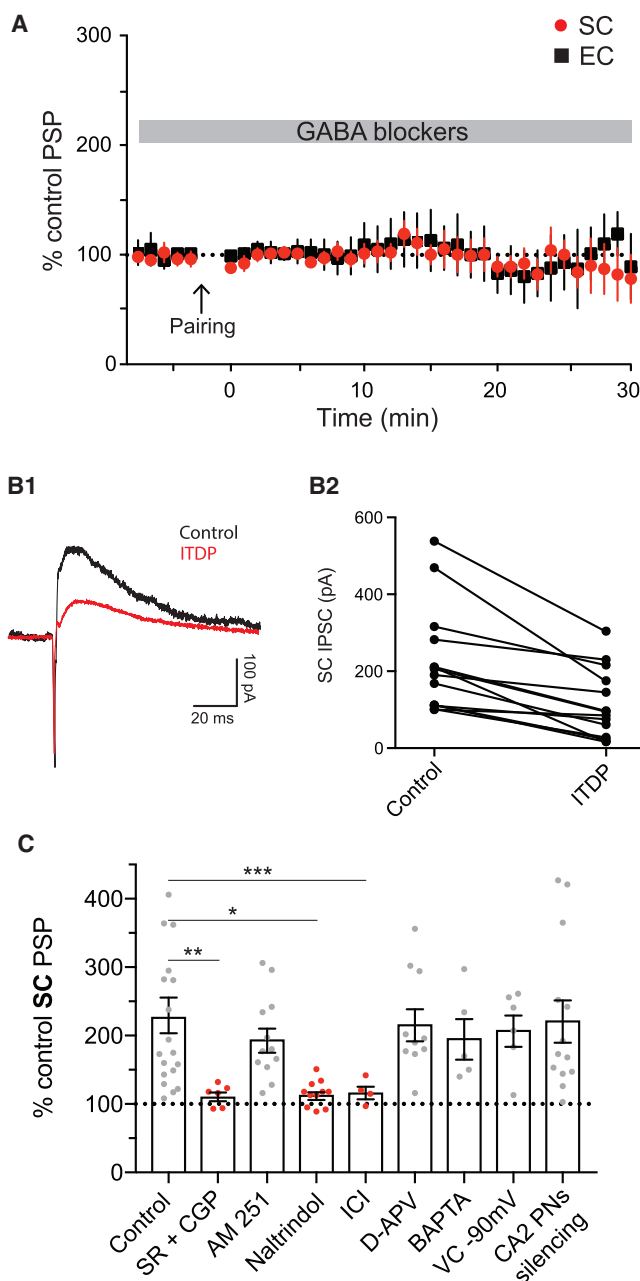


Figure 2. Mechanisms of ITDP in CA2 PNs

(A) Time course of the average normalized PSP amplitudes obtained in whole-cell current clamp following ITDP induction in the presence of GABA blockers. (B) Whole-cell voltage-clamp recordings of CA2 PNs IPSCs at a holding potential of -10 mV. IPSCs are induced by SC stimulation (B1). Amplitude of the SC IPSCs is compared before and after ITDP (B2). (C) Normalized SC PSP amplitudes following ITDP induction in the presence of different drugs or with the CA2 PNs silenced by inhibitory DREADDs. Data are represented as mean \pm SEM. See also Figure S2.

to findings in CA1 (Basu et al., 2013). However, the extent of CA2 ITDP at -10 and -30 ms intervals ($145\% \pm 16\%$ and $150\% \pm 20\%$, respectively) was greater than typically observed in CA1

(120% and 135% , respectively), indicating that CA2 ITDP is less narrowly tuned to the -20 ms interval. Nonetheless, CA2 ITDP was still significantly greater using a -20 ms pairing interval compared to other intervals (Mann-Whitney test, $p = 0.03$ and $p = 0.04$ compared to -10 ms and -30 ms intervals, respectively).

CA2 ITDP Results from LTD of the IPSP through Activation of δ -Opioid Receptors, whereas CA1 ITDP Involves iLTD of Cholecystinin-Positive INs

The majority of the increase in the SC-evoked PSP during ITDP in CA1 is caused by iLTD, resulting in a larger net synaptic depolarization (Basu and Siegelbaum, 2015). As robust iLTD in CA2 PNs can be induced by tetanic stimulation of the SC or EC inputs to CA2 (Nasrallah et al., 2015, 2017; Piskorowski and Chevaleyre, 2013), we examined the role of iLTD in CA2 ITDP. Application of GABA_A and GABA_B receptor antagonists ($2 \mu\text{M}$ SR 95531 and $1 \mu\text{M}$ CGP 55845, respectively) throughout the experiment fully blocked ITDP at both the SC inputs (PSP remained at $102\% \pm 8\%$ of baseline, $n = 8$; Wilcoxon test, $p = 0.9$ compared to baseline) and EC inputs (PSP remained at $107\% \pm 23\%$ of baseline, $n = 7$; Wilcoxon test, $p = 0.9$ compared to baseline; Figures 2A and 2C). These results indicate that the expression of CA2 ITDP is due solely to iLTD, which differs from CA1 where, in addition to iLTD, ITDP recruits a 40% long-term potentiation of the SC excitatory postsynaptic potential (EPSP; Basu et al., 2013). The lack of eLTP in CA2 is consistent with findings that tetanic stimulation of the SC inputs also fails to induce conventional LTP in CA2 (Dudek et al., 2016).

To directly test whether ITDP results from a decrease in inhibitory synaptic transmission, we recorded the feedforward inhibitory postsynaptic current (IPSC) in CA2 PNs elicited by stimulation of the SC inputs under voltage-clamp conditions. We held the membrane at -10 mV to increase the outward driving force on the IPSC and reduce the excitatory postsynaptic current driving force (Figure 2B1). The ITDP induction protocol significantly decreased the IPSC to $48\% \pm 11\%$ of its initial level ($n = 14$; Wilcoxon test, $p = 0.0001$ compared to baseline; Figure 2B2), similar to the effects of ITDP on the IPSC seen in CA1 (Basu et al., 2013), directly demonstrating the contribution of iLTD to the expression of CA2 ITDP.

Next, we examined whether the cellular and molecular mechanisms underlying ITDP in CA2 were similar to those previously described for ITDP in CA1, in which iLTD results from a selective decrease in feedforward inhibition mediated by CCK⁺ basket cells through activation of endocannabinoid CB1 receptors (Basu et al., 2013; Xu et al., 2012). However, unlike ITDP in CA1, application of the CB1R antagonist AM251 ($2 \mu\text{M}$) had no effect on the magnitude of CA2 ITDP ($196\% \pm 16\%$, $n = 12$; Wilcoxon test, $p < 0.001$ compared to baseline; Figure 2C).

Previous studies reported that CA2 iLTD induced by high-frequency tetanic stimulation of the SC inputs is mediated by the activation of δ -opioid receptors (Piskorowski and Chevaleyre, 2013), which suppress inhibitory synaptic transmission mediated by PV⁺ INs (Svoboda et al., 1999). We found that a similar mechanism contributes to iLTD induced during ITDP in CA2. Using immunohistochemical labeling, we found that δ -opioid receptors were expressed specifically by CA2 PV⁺ INs (Figure S2) in mouse hippocampus, which is somewhat different from the

rat hippocampus where CA2 PNs also express δ -opioid receptors (Burstein et al., 2013). Importantly, we found that bath application of both peptide (2 μ M ICI 174,864) and non-peptide (0.1 μ M naltrindole) antagonists of δ -opioid receptors fully blocked ITDP (Figure 2C). 30 min after delivery of the ITDP induction protocol, the SC PSP remained at $106\% \pm 5\%$ of its baseline level with naltrindole present ($n = 11$; Wilcoxon test, $p = 0.2$ compared to baseline) and $102\% \pm 13\%$ of baseline with ICI 174,864 ($n = 5$; Wilcoxon test, $p = 0.9$ compared to baseline).

Another hallmark of iLTD induced during ITDP in CA1 is that it shares certain mechanisms with eLTP, requiring activation of NMDA receptors and postsynaptic depolarization. However, blocking NMDA receptors with 50 μ M D-2-amino-5-phosphonovaleate (D-APV) had no effect on the magnitude of ITDP in CA2 ($218\% \pm 23\%$, $n = 11$; Wilcoxon test, $p = 0.002$ compared to baseline; Figure 2C). Additionally, chelation of intracellular Ca^{2+} by inclusion of 20 mM BAPTA in the CA2 PN patch pipette failed to inhibit CA2 ITDP ($198\% \pm 30\%$, $n = 5$; Wilcoxon test, $p = 0.002$ compared to baseline; Figure 2C), in contrast to its ability to block CA1 ITDP (Basu et al., 2013). Delivery of the ITDP induction protocol with the CA2 PN voltage clamped at -90 mV, which prevents Ca^{2+} influx through the NMDA receptors, also failed to block ITDP ($210\% \pm 23\%$, $n = 6$; Wilcoxon test, $p = 0.03$ compared to baseline; Figure 2C), although it blocks ITDP in CA1 (Basu et al., 2013).

The above results clearly show that cell-autonomous CA2 PN activity is not necessary for ITDP. However, it is possible that activity in neighboring CA2 PNs may provide a transcellular messenger to induce ITDP in a nearby inactivated neuron. To investigate this possibility, we inhibited the entire CA2 PN population by expressing and activating the hM4Di inhibitory DREADD receptor (iDREADD; Urban and Roth, 2015) specifically in CA2 PNs. We injected a Cre-dependent rAAV vector expressing hM4Di into the CA2 region of adult Amigo2-Cre mice, which limits Cre expression to CA2 PNs (Hitti and Siegelbaum, 2014). Although application of the specific hM4Di ligand clozapine N-oxide (CNO; 5 μ M) to hippocampal slices from mice expressing hM4Di caused a significant hyperpolarization of CA2 neurons (Figures S2C and S2D), it failed to reduce ITDP ($224\% \pm 31\%$, $n = 13$, Wilcoxon test, $p = 0.0002$ compared to baseline; Figure 2C), arguing against a role for general CA2 PN activity. Thus, although ITDP in CA1 and CA2 both involve iLTD, their cellular and molecular mechanisms differ markedly.

Expression of CA2 ITDP Results from LTD of the IPSP from PV⁺ INs

To explore the involvement of PV⁺ INs in CA2 ITDP, we examined the effect of silencing these neurons using a pharmacogenetic approach. We injected mice expressing Cre selectively in PV⁺ INs (PV-Cre mice; Hippenmeyer et al., 2005) with a rAAV expressing iDREADD in a Cre-dependent manner (Figure 3A) and performed experiments 3 weeks later in acute hippocampal slices. We observed sparse expression of iDREADD throughout the hippocampus, notably in the CA2 region around the end of the mossy fiber pathway (arrowhead in Figure 3E1). Expression of iDREADD was confined to the PV⁺ INs as shown by co-labeling for iDREADD and PV (Figure 3E). Application of 5 μ M CNO to hippocampal slices from mice expressing iDREADD decreased

both the EC- and SC-evoked IPSCs (EC IPSC decreased by $22\% \pm 4\%$ and SC IPSC decreased by $35\% \pm 6\%$; $n = 8$, Wilcoxon test, $p = 0.008$ compared to baseline in both cases; Figure S3A). As PV⁺ IN-mediated inhibition accounts for approximately 50% of the total feedforward inhibition activated by the SC pathway (Piskorowski and Chevaleyre, 2013), iDREADD activation silenced about 70% of PV-mediated feedforward inhibition in these experiments.

To determine the contribution of PV⁺ INs to ITDP, we examined ITDP in slices when PV⁺ INs expressing iDREADD were silenced by continuous perfusion with CNO (Figures 3B and 3C). Although normal levels of ITDP were observed in recordings from CA2 PNs in slices from wild-type (WT) mice injected with Cre-dependent iDREADD rAAV (controls, ITDP = $187\% \pm 16\%$, $n = 8$), ITDP was largely blocked in slices from PV-Cre mice expressing iDREADD (ITDP = $115\% \pm 13\%$, $n = 17$; Mann-Whitney test, $p = 0.03$ for control versus PV-iDREADD; Figures 3C, 3D, and 3F).

PV⁺ INs Are Required for Expression, but Not Induction, of ITDP

Next, we asked whether activation of the PV⁺ IN population was required for the induction of ITDP by specifically silencing these neurons only during the 90 s pairing protocol. As CNO washout is too slow to selectively silence neurons only during this period, we used an optogenetic approach by injecting a Cre-dependent rAAV in CA2 of PV-Cre mice to express YFP-tagged Arch3.0-YFP, an inhibitory opsin, in local PV⁺ INs (Figure S4A). As with iDREADD viral injection, expression of Arch3.0-YFP was confined to PV⁺ INs, with YFP-labeled cells and terminals prominently observed in the CA2 region defined using the PCP4 marker (Figure S3E).

Before inducing ITDP, we first tested the ability of Arch3.0-YFP photo-activation to suppress feedforward inhibition. A 500 ms light pulse at maximum intensity caused a significant reduction in the IPSC evoked by electrical stimulation of either EC ($27\% \pm 7\%$ reduction, $n = 7$; Wilcoxon test, $p = 0.03$ compared to baseline) or SC ($37\% \pm 3\%$ reduction, $n = 15$; Wilcoxon test, $p = 0.0002$ compared to baseline; Figure S3B) inputs, indicating that Arch3.0 activation blocked 50%–75% of feedforward inhibition mediated specifically by the PV⁺ INs.

Next, we applied a more prolonged period of photo-stimulation to inhibit PV⁺ IN activity during the entire 90 s period of the ITDP pairing protocol (Figure S4B1). Despite the continuous photo-activation of Arch3.0-YFP (which silences neurons more efficiently than a brief light pulse; Chow et al., 2010), the pairing protocol still induced a large ITDP, with the SC PSP increasing to $245\% \pm 33\%$ of baseline ($n = 13$; Figure S4C), similar to that in control slices not expressing Arch3.0-YFP (PSP increased to $229\% \pm 26\%$ of baseline, $n = 19$; Mann-Whitney test, $p = 0.7$ control versus Arch3.0-YFP slices; Figure S4D). Prolonged Arch3.0-mediated inhibition of the PV⁺ INs also failed to suppress ITDP of the EC PSP. In the Arch3.0-YFP group, the PSP increased to $163\% \pm 25\%$ of baseline ($n = 7$), similar to the $138\% \pm 13\%$ increase in controls ($n = 17$; Mann-Whitney test, $p = 0.5$; Figure S4D). Therefore, we conclude that PV⁺ INs are necessary for the expression of ITDP but do not need to be activated during the pairing protocol for the induction of ITDP.

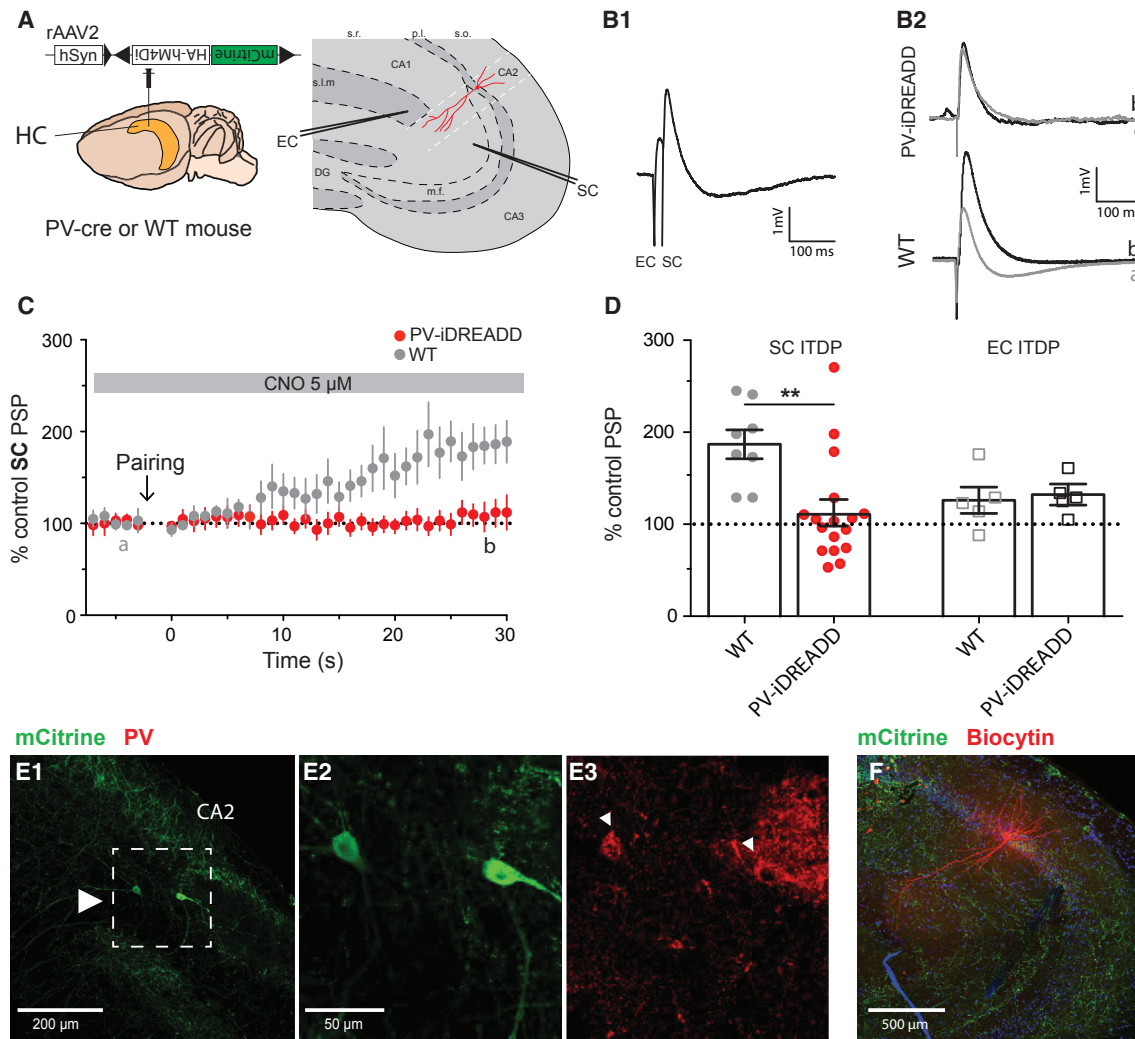


Figure 3. PV+ IN Population Is Necessary for ITDP Expression

(A) Experimental design showing injection of Cre-dependent iDREADD virus in PV-Cre or WT mouse.

(B) PSPs recorded in whole-cell current-clamp configuration in response to paired electrical stimulation of EC+SC inputs (B1) or SC inputs alone (B2) from neurons in slices from PV-Cre mouse expressing iDREADD or WT mouse injected with same virus (no iDREADD expression); 5 μ M CNO was present throughout experiment. Example paired EC+SC PSPs from CA2 PN in iDREADD-expressing slice (B1). SC-evoked PSPs before (black) and 30 min after (gray) ITDP induction (B2).

(C) Time course of mean \pm SEM SC PSP amplitude during ITDP.

(D) SC (filled circles) and EC (open squares) PSP amplitude following ITDP induction using electrical pairing in WT or PV-Cre mice, both injected with iDREADD. Symbols show data for single cells; bars show mean \pm SEM.

(E) Immunohistochemistry of acute hippocampal slice showing mCitrine (from Cre-dependent virus) and PV expression at low (E1) and high (E2 and E3) magnification.

(F) Immunohistochemistry of acute hippocampal slice showing mCitrine and biocytin-filled neuron. See also Figures S3 and S4.

These optogenetic experiments also provided an independent means of assessing the extent to which ITDP reduces PV-mediated feedforward inhibition. Photo-activation of Arch3.0-YFP reduced the SC-evoked IPSC amplitude by $30.6\% \pm 3.5\%$ before induction of ITDP but caused only an $8.9\% \pm 1.8\%$ decrease in IPSC amplitude after induction of ITDP ($n = 12$, Wilcoxon test, $p = 0.0002$ before versus after ITDP; Figure S3C). These results suggest that ITDP reduces the PV⁺ IN-mediated IPSC to less than 30% of its initial level ($100\% \times 8.9/30.7$), providing further evidence that ITDP expression results from a decrease in PV⁺ IN-mediated feedforward inhibition.

CA2 ITDP Requires Paired Activation of SC and EC Layer II Stellate Cell Inputs

Previous studies have shown that layer II (LII) neurons in medial and lateral entorhinal cortex (MEC and LEC) send excitatory projections to CA2 PNs through SLM (Hitti and Siegelbaum, 2014; Kohara et al., 2014). As projections from other brain regions may also be present in SLM, we used optogenetic stimulation of defined EC inputs to confirm that pairing of these inputs with SC stimulation is sufficient to induce ITDP.

We injected a rAAV vector that expressed channelrhodopsin-2 tagged with YFP under control of the CaMKII promoter

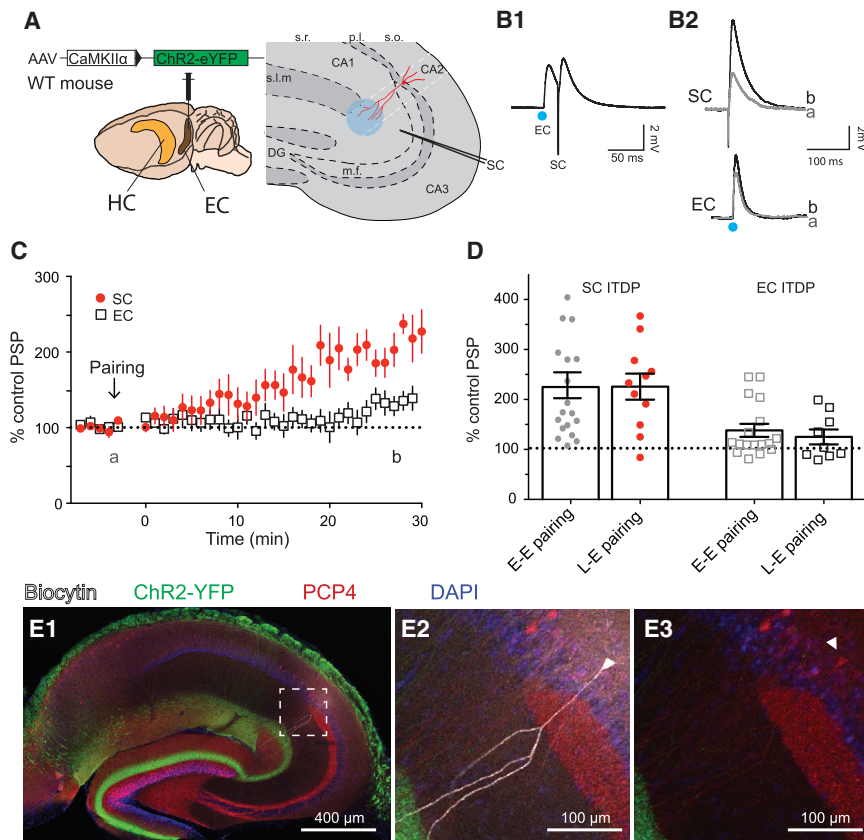


Figure 4. Pairing Light Stimulation of the MEC Excitatory Inputs with SC Stimulation Also Induces ITDP in CA2

(A) Experimental design of the experiment and injection site of the channelrhodopsin-expressing virus.

(B) Responses obtained in whole-cell current-clamp configuration using light (EC) or electrical (SC) stimulations during ITDP induction (B1; EC+SC pair); SC and EC PSPs before (black) and 30 min after (gray) ITDP induction (B2).

(C) Time course of PSP amplitudes during ITDP. (D) Normalized SC (filled circles) and EC (open squares) PSP amplitudes following ITDP induced using electrical-electrical (E-E) or light-electrical (L-E) pairing. Symbols show data for single cells; bars show mean \pm SEM.

(E) Immunohistochemistry of the acute hippocampal slice against biocytin, ChR2-YFP, PCP4. Arrowhead in (E3) indicates the PCP4-positive soma of the recorded cell. Data from (B) and (E) are from the same CA2 PN. See also Figure S5.

(ChR2-EYFP; Figure 4A) into superficial layers of MEC, resulting in specific expression of ChR2-EYFP in excitatory neurons in superficial MEC (Figure S5). 2 weeks after the injection, we used 1 ms light pulses to photo-stimulate the EC inputs, which evoked PSPs in CA2 PNs recorded from acute hippocampal slices (Figure 4B). After the experiment, we fixed the slices and stained for YFP, biocytin, and PCP4 to confirm the expression pattern of EC fibers and the identity of the recorded cell (Figure 4E).

Pairing a 1 ms light pulse followed by electrical stimulation of the SC inputs after a 20 ms delay for 90 s at 1 Hz produced a robust ITDP of the SC-evoked PSP (Figure 4B). The peak SC-evoked depolarization measured 30 min after the pairing protocol increased to $225\% \pm 25\%$ of baseline ($n = 11$; Figure 4C), identical to that seen when ITDP was induced by paired electrical stimulation ($229\% \pm 26\%$, $n = 19$; Mann-Whitney test, $p = 0.9$ compared to photo-stimulation-induced ITDP; Figure 4D). The EC PSP also showed a moderate increase ($130\% \pm 23\%$, $n = 5$; Figure 4C), similar to that seen with paired electrical stimulation ($138\% \pm 13\%$, $n = 17$; Mann-Whitney test, $p = 0.4$ compared to photo-stimulation-induced ITDP; Figure 4D). Thus, we conclude that pairing of MEC excitatory inputs to CA2 with SC stimulation is sufficient to induce ITDP.

Direct Entorhinal Cortex Inputs to CA2 PNs Originate from LII Stellate Cells

Next, we sought to identify the excitatory neuronal population in EC that projects to CA2 and is responsible for the induction of

ITDP. EC LII contains a mixed population of Reelin-positive stellate cells and calbindin-1-positive PNs (Kitamura et al., 2014). To determine which of these neurons form synapses with CA2 PNs, we carried out retrograde tracing experiments by co-injecting the G-deleted SB19 strain of rabies virus (Wall et al., 2010) with Cre-dependent helper virus in the CA2 region of Amigo2-Cre mice (Figure 5A).

10 days after injection of the GFP-expressing virus in the dorsal CA2 region of Amigo2-Cre mice (Hitti and Siegelbaum, 2014), we stained cortical slices for GFP, Reelin, and calbindin-1. We observed a preponderance of retrogradely labeled GFP-expressing cells in LII of the MEC as well as a few cells in deep layers IV and V (Figure 5B; see also Figure S6A for CA2 specificity of primary infection). Double staining for Reelin and calbindin-1 in LEC revealed that every GFP-positive LII neuron also expressed Reelin, but not calbindin-1 (Figure 5C). Thus, we conclude that CA2 PNs receive input from EC LII stellate cells, the same class of neurons that project to DG and CA3. We confirmed these results using the more efficient N2C strain of rabies virus (Reardon et al., 2016).

The above results demonstrate that, within the EC, only LII stellate cells project to CA2 PNs. However, it is possible that ITDP requires input from a different class of EC neurons that project to CA2 but form synapses on interneurons. Such neurons would not be labeled by the rabies virus under the above conditions. To directly confirm the importance of the LII stellate cells for ITDP, we expressed ChR2 in these neurons specifically and paired light stimulation with electrical activation of the SC inputs. As we lacked a stellate-cell-specific Cre line, we used a dual viral injection strategy. We first injected a canine adenovirus 2 vector that expresses Cre (CAV2-Cre) into the DG. 2 weeks later, we injected a Cre-dependent ChR2-YFP virus into LEC. As CAV2-Cre travels retrogradely and is monosynaptic, it will only lead to Cre expression in neurons presynaptic to the DG (Junyent and

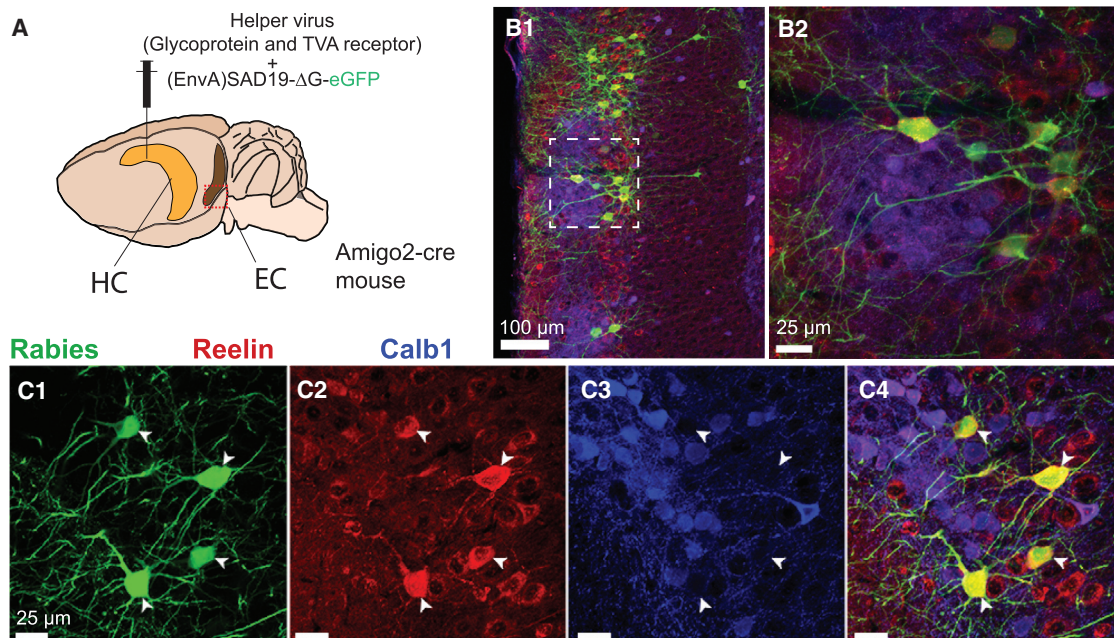


Figure 5. CA2 Direct EC Inputs Originate from the EC LII Stellate Cells

(A) Experimental design and injection site of the helper and rabies viruses.

(B and C) Immunohistochemistry of the MEC (B) and LEC (C) against rabies-YFP, Calb1, and Reelin. See also Figure S6.

Kremer, 2015). Given that the only EC inputs to the DG are from LII stellate cells, CAV2-Cre should be expressed specifically in these neurons in EC. To verify the efficacy of this strategy, we injected CAV2-Cre in the DG of an Ai14 reporter mouse line, which allows for tdTomato expression in neurons expressing Cre. 10 days after injection we found that nearly all tdTomato⁺ neurons were EC LII stellate cells and expressed the stellate marker Reelin, but not the EC LII PN marker calbindin-1 (Figure S7).

Having verified the specificity of this approach, we repeated the CAV2-Cre injections into the DG of WT animals and 2 weeks later injected a Cre-dependent Chr2-YFP virus into the LEC (Figure 6A). The resultant Chr2-YFP signal was present in a pattern consistent with the expected localization to LEC LII stellate cell projections (Kohara et al., 2014). Photo-stimulation successfully evoked a depolarizing PSP in most CA2 PNs (Figure 6B). Moreover, pairing light with SC electrical stimulation induced a robust ITDP similar to that seen with paired electrical stimulation (Figures 6B and 6C). Thus, the SC response was increased to 208% ± 18% of baseline (n = 18) compared to 229% ± 26% (n = 19) with electrical stimulation (Mann-Whitney test, p = 0.9; Figure 6D). This protocol also induced ITDP of the light-evoked EC LII stellate cell PSP (130% ± 15%, n = 16, versus 138% ± 13%, n = 17, for electrical stimulation; Mann-Whitney test, p = 0.7; Figure 6D).

As discussed above, CA2 ITDP does not appear to require postsynaptic depolarization of the CA2 PN during the pairing protocol. We were able to specifically demonstrate that the presence of an EC-evoked PSP in CA2 PNs is not required for the induction of ITDP by examining a subset of recordings in which photo-stimulation of the LII EC inputs failed to evoke a noticeable depolarizing PSP in the patch-clamped CA2 PN, even though there was strong expression of Chr2-GFP in fibers extending to CA2 in

the same slice (same pattern as in Figure 6E1). The absence of a photo-stimulated PSP was not a result of our having severed the distal dendrites during slice preparation as the same CA2 PNs displayed a normal-sized EC PSP with distal electrical stimulation. Rather, the absence of the PSP likely reflects heterogeneity in innervation of individual CA2 PNs by Chr2-expressing axons from EC. Surprisingly, the pairing protocol induced a large ITDP in the electrically evoked SC PSP in the same CA2 PNs that failed to generate an EPSP in response to EC photo-stimulation (PSP increased to 230% ± 23% of baseline, n = 6, for photo-stimulation versus 229% ± 26%, n = 19, for electrical stimulation; Mann-Whitney test, p = 0.6; Figure 6D). We also saw a normal-sized ITDP in the electrically evoked EC PSP (151% ± 21% for ITDP from non-photo-responsive cells, n = 5, versus 138% ± 13% for ITDP induced electrically, n = 17; Mann-Whitney test, p = 0.5; Figure 6D). These results strongly support the idea that the induction of ITDP does not require that the CA2 PN itself be activated during the ITDP pairing protocol (Figure 2C).

Sites of Enkephalin Release in CA2

What is the site of enkephalin release required for the induction of CA2 iLTD and ITDP? Interestingly, enkephalins have been detected in interneurons that synapse onto other interneurons (Blasco-Ibáñez et al., 1998; Commons and Milner, 1996), including those synapsing onto PV⁺ basket cells (Fuentelba et al., 2008). We screened a number of enkephalin antibodies and identified two that provided a consistent pattern of staining. Enkephalin was found in a number of presynaptic terminals and pathways that impinged on CA2, including dentate gyrus granule cell mossy fiber inputs to CA3 and CA2 (arrowhead in Figure 7A), as previously reported (Chavkin et al., 1983, 1985; Gall et al., 1981;

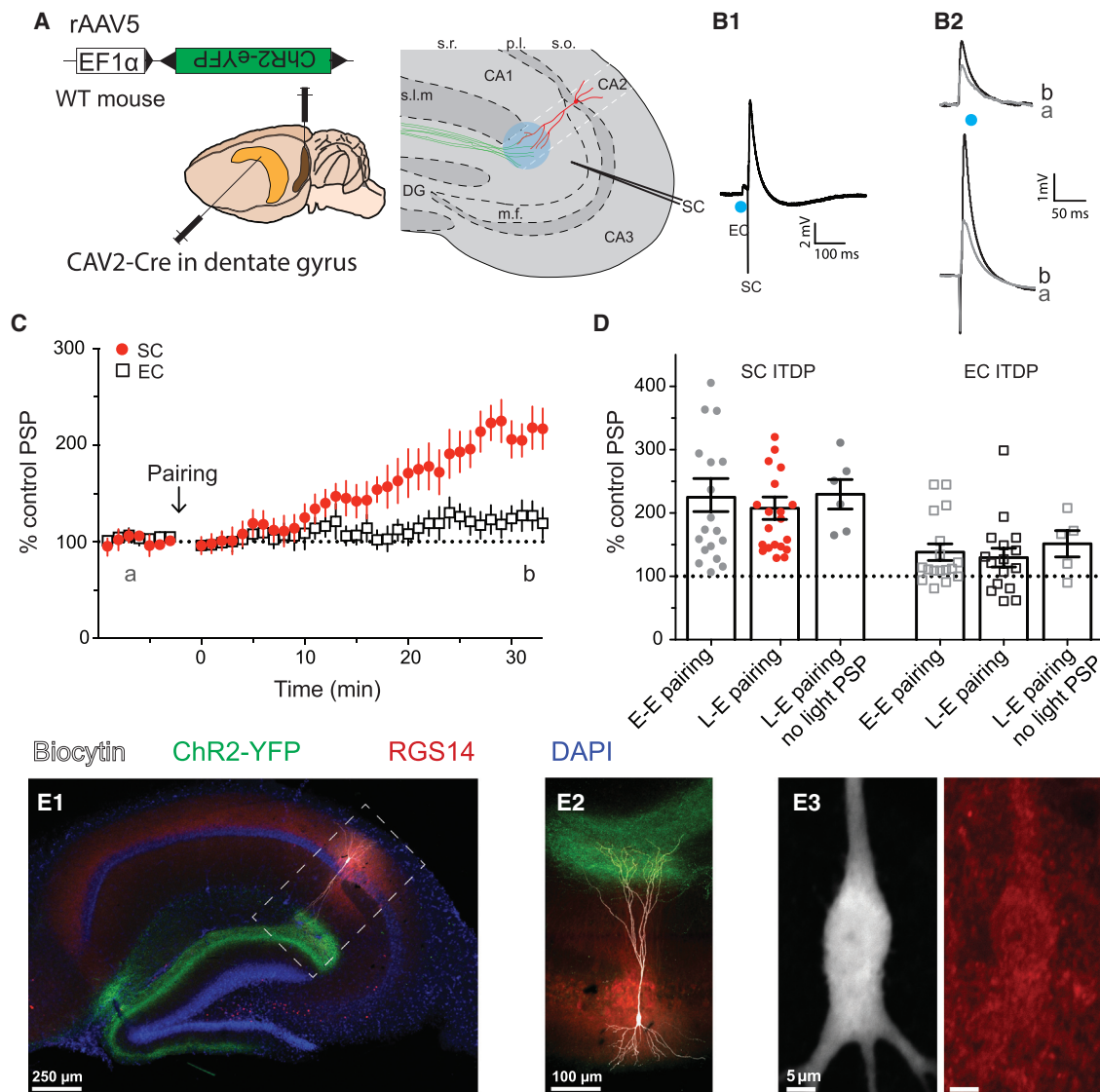


Figure 6. Pairing Photo-stimulation of LEC LII Stellate Cells Inputs with SC Electrical Stimulation Induces ITDP in CA2

(A) Experimental design and injection sites of CAV2-Cre in DG and Cre-dependent ChR2 rAAV in EC.

(B) CA2 PN PSPs from whole-cell current-clamp recordings. PSPs evoked using paired light (EC) and electrical (SC) stimulation during ITDP induction (B1). Light-evoked EC PSPs (top) and electrically evoked SC PSPs before (black) and 30 min after (gray) ITDP induction (B2).

(C) Time course of mean \pm SEM peak PSP amplitude during ITDP.

(D) SC (filled circles) and EC (open squares) PSP amplitudes normalized by baseline showing ITDP induced by pairing electrical stimulation of the SC input with electrical (E-E) or light (L-E) stimulation of the EC input. Results for ITDP in cells that showed no light-evoked EC PSP are also shown (L-E pairing, no light PSP). Symbols show data for single cells; bars show mean \pm SEM.

(E) Immunohistochemistry from hippocampal slices against YFP, biocytin, and RGS14. Whole slice (E1). Expanded view of the recorded cell morphology (E2). High-magnification view of the soma of the recorded cell (left, biocytin image) to confirm the expression of the CA2 marker RGS14 (right, red) (E3). See also Figure S7.

McGinty et al., 1983; Terrian et al., 1988). We also observed staining surrounding CA2 PN soma (Duka et al., 1981). Double labeling for enkephalin and PV also revealed prominent staining for enkephalin surrounding PV⁺ IN soma located in or near the CA2 PN cell body layer (Figures 7B and 7C). Although these results indicate the presence of enkephalin-positive (ENK⁺) neurons in the CA2 region, the specific neuronal population that releases enkephalin for the induction of ITDP remains unknown.

Blockade of δ -Opioid Receptors within CA2 Inhibits Social Memory Behavior

What functional role might CA2 ITDP, or its underlying plasticity mechanism of iLTD, play in hippocampal-dependent learning and memory? Previous studies have implicated CA2 in social memory (Hitti and Siegelbaum, 2014; Stevenson and Caldwell, 2014), whereas ITDP in CA1 has been proposed to enhance the specificity and strength of contextual and object memory

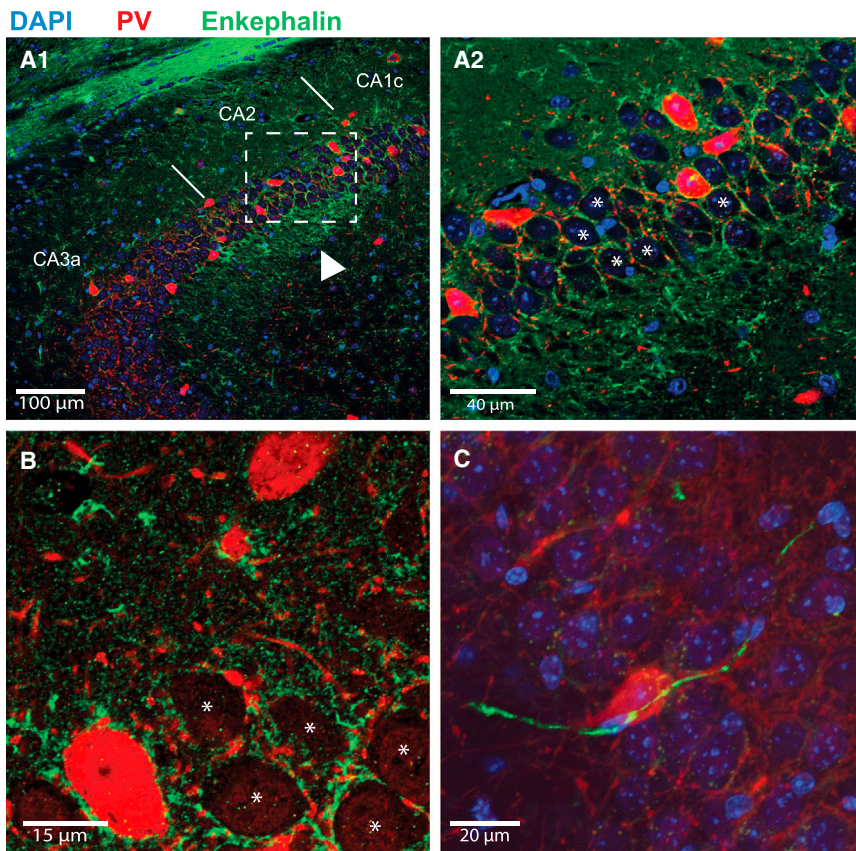


Figure 7. ENK⁺ Fibers Contact PV⁺ INs

(A–C) Immunohistochemistry of the hippocampus with antibodies recognizing PV (red) and enkephalin (green). Fitzgerald enkephalin antibody used in (A) and (B); Santa Cruz enkephalin antibody used in (C); see STAR Methods. Arrowhead in (A1) points to the end of the mossy fiber pathway. (A2) Higher-magnification view of dashed box region in (A1). High-magnification view of the tight network of ENK⁺ (green) and PV⁺ fibers (red) surrounding unstained CA2 PNs somas (asterisks) (B). Two PV⁺ neuron somas are also seen (large red somas). In (C), an ENK⁺ fiber can be seen impinging on a PV⁺ soma.

(Basu et al., 2016). As activation of δ -opioid receptors is required for both ITDP (Figure 2C) and iLTD (Piskorowski and Chevaleyre, 2013), we explored the effect on social memory of infusion of a specific δ -opioid receptor antagonist through a cannula targeting CA2. Although drug infusion lacks the specificity of genetic inactivation, long-lasting effects of bath application of the δ -opioid receptor-selective agonist DPDPE to hippocampal slices are restricted to CA2. Thus, DPDPE selectively induces iLTD of PV⁺ IN-mediated feedforward inhibition in CA2 PNs (Piskorowski and Chevaleyre, 2013) while causing only a transient decrease of feedforward inhibition in neighboring CA1 neurons (Piskorowski and Chevaleyre, 2013). Moreover, we found that δ -opioid receptor activation had no effect on inhibition or excitation in CA3 (Figure S8A). The finding that δ -opioid receptor signaling has a selective long-lasting action in CA2, but not in surrounding CA1 or CA3 regions, implies that any behavioral effects of *in vivo* infusion of a δ -opioid receptor antagonist into the CA2 region likely results from its actions within CA2.

We explored the role of CA2 δ -opioid receptors in social memory by implanting 3-month-old WT animals with bilateral cannulas targeting CA2. We then perfused 1 μ L of the δ -opioid receptor antagonist naltrindole (5 mM solution) in CA2 30 min before performing a direct interaction test of social memory (Figure 8A; Kogan et al., 2000). In this test, the subject mouse is allowed to interact with a novel juvenile mouse for two 2 min trials separated by a 30 min inter-trial interval (Figure 8A). Social memory is evidenced by the lower interaction time in trial 2 compared to

trial 1. In saline-infused control animals, the average interaction time was 58 ± 5 s during the first trial, and it decreased to 24 ± 4 s during the second trial, indicative of social memory ($n = 9$; Wilcoxon test, $p = 0.004$ compared to baseline; Figure 8B; Movie S1). Although naltrindole-infused animals also showed a decrease in interaction time from trial 1 (52 ± 4 s) to trial 2 (36 ± 5 s; $n = 9$; Wilcoxon test, $p = 0.01$ compared to baseline; Figure 8B; Movie S2), the percent reduction in the drug-treated group ($31\% \pm 8\%$, $n = 9$) was significantly smaller than the reduction in the control group ($60\% \pm 7\%$, $n = 9$; Mann-Whitney test, $p = 0.008$; Figure 8C).

After the experiment, we perfused each animal with 1 μ L of the dye mini-Ruby (5 mM solution) to verify the location of the perfusion (Figure 8D). For all animals included in the analysis, the dye was largely co-labeled with the CA2 marker RGS14, with a modest extent of dye leakage in CA3a or CA1c regions adjacent to CA2, areas that do not show long-term δ -opioid receptor actions.

Social Interactions that Engage Social Memory Occlude ITDP and Reduce Feedforward Inhibition

Next, we asked whether social interactions with a novel animal that lead to social memory storage are able to recruit ITDP (or a related plasticity process). To explore this possibility, we performed an occlusion experiment to determine whether direct social interaction of an adult male subject mouse with a novel juvenile mouse for 2 min was sufficient to reduce the magnitude of ITDP in slices prepared from the subject mouse within 45 min of the interaction. Indeed, the amount of potentiation of the SC PSP following induction of ITDP was significantly reduced in slices obtained from mice that received a novel social stimulus (PSP was increased to $122\% \pm 6\%$ of baseline, $n = 9$) compared to slices obtained from mice exposed to a littermate for 2 min (PSP was increased to $229\% \pm 26\%$ of baseline, $n = 19$; Mann-Whitney test, $p = 0.0007$; Figure 8E). The reduction in ITDP after a novel social interaction suggests that this experience was able to recruit CA2 ITDP, thereby occluding further potentiation in the slice recordings.

If social interaction between a subject mouse and a novel animal does indeed recruit either ITDP or a related plasticity

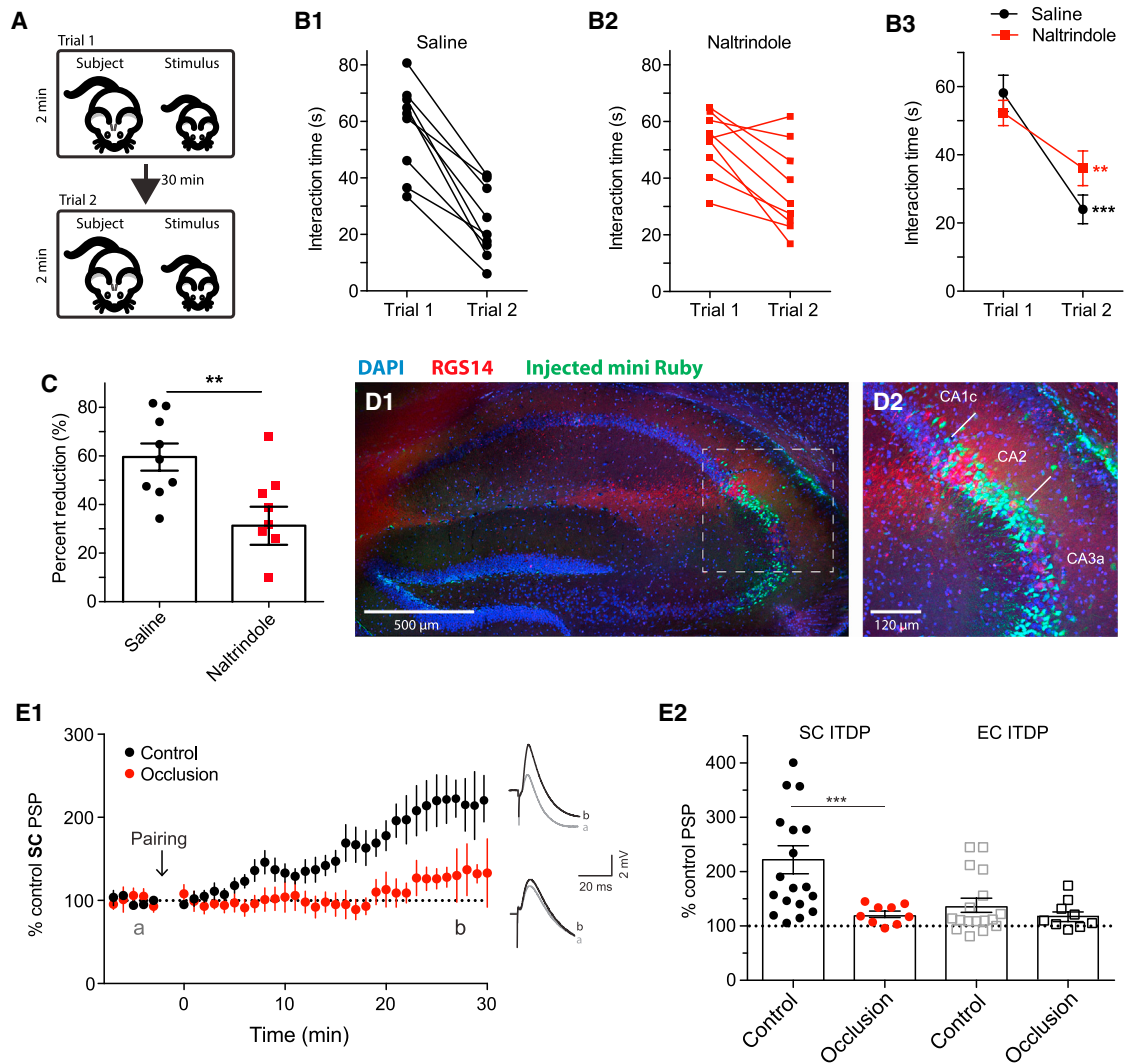


Figure 8. δ -opioid receptor Blockade in CA2 Reduces Social Memory and Social Memory Occludes ITDP

(A) Schematic of the direct interaction test for social memory.

(B) Interaction time of saline (B1) and naltrindole-injected (B2) animals in trials 1 and 2 (symbols from individual animals) and superimposed mean \pm SEM (B3).

(C) Percent reduction of interaction time from trial 1 to trial 2.

(D) Mini-Ruby infusion in the hippocampus and immunohistochemistry for RGS14.

(E) Time course of mean \pm SEM normalized SC PSP amplitude obtained in whole-cell current clamp following ITDP induction. Slices were prepared from mice that either experienced a 2 min interaction with a novel juvenile male (social novelty) or were continuously housed with littermates (social familiarity). Note pronounced reduction in ITDP in response to social novelty (D). ITDP of PSPs evoked by stimulation of SC (filled circles) or EC (open squares) inputs to CA2 PNs in slices from indicated groups of animals. Symbols show data for single cells; bars show mean \pm SEM. See also Figure S8.

process that is able to induce iLTD, then the amount of feedforward inhibition should also be reduced in slices obtained from a subject mouse soon after its interaction with a novel mouse. To explore this possibility, we compared the size of the IPSC recorded from CA2 neurons in response to SC stimulation in slices obtained from mice exposed to a novel animal for 2 min (experimental group) compared to slices from control mice exposed to a littermate for 2 min (three mice and ten cells for each condition). The amount of feedforward inhibition recorded in CA2 PNs was indeed significantly smaller in slices prepared from the experimental group compared to slices from the control

group (ANOVA novelty factor $F_{(1,237)} = 50.72$, $p < 0.0001$, Figure S8B). Thus, both our behavioral and slice electrophysiology experiments support the idea that δ -opioid receptors in CA2 may regulate the strength of social memory through induction of ITDP or a closely related mechanism.

DISCUSSION

We report that CA2 PNs exhibit a robust increase in the magnitude of the peak depolarization of the SC-evoked PSP in response to paired activation of their EC and SC inputs. In many respects,

this plasticity is similar to ITDP in CA1 (Dudman et al., 2007). Similar to CA1 ITDP, CA2 ITDP was induced by low-frequency, subthreshold pairing of EC and SC inputs that failed to elicit CA2 action potentials. Moreover, ITDP in CA2 was maximal when the SC inputs were activated 20 ms after the EC inputs, similar to the timing dependence of ITDP in CA1. Finally, as in CA1 (Basu et al., 2013), the increase in the net PSP in CA2 depends on iLTD.

However, in a number of other respects, ITDP in CA2 differs from that in CA1. Whereas ITDP in CA1 is driven by EC layer III (LIII) PN projections to CA1 distal dendrites, ITDP in CA2 requires input from EC LII stellate cells. CA1 and CA2 ITDP also differ in their molecular mechanisms. Thus, ITDP and iLTD in CA2 require activation of δ -opioid receptors, which selectively regulate feedforward inhibition mediated by PV⁺ INs. In contrast, ITDP in CA1 depends on activation of endocannabinoid CB1 receptors, which suppress inhibition mediated by CCK⁺ INs. In addition, whereas CA1 ITDP requires postsynaptic depolarization, NMDA receptor activation and dendritic integration of the EC and SC inputs by the CA1 PN (Basu et al., 2016), CA2 ITDP does not require CA2 PN depolarization or NMDA receptor activation. This suggests that the site of integration of CA2 ITDP lies outside of the CA2 PN. Finally, ITDP is more precisely tuned to the 20 ms pairing interval in CA1 compared to CA2. This may reflect the differential contribution of long-range inhibitory projections from EC, which enable CA1 ITDP induction by suppressing a population of dendrite-targeting CA1 INs. These inputs do not project to CA2 (Basu et al., 2016).

The Differential Role of δ -Opioid Receptor-Dependent Inhibition of PV⁺ IN CA2 ITDP

The mechanism underlying ITDP in CA2 resembles δ -opioid receptor-dependent iLTD induced by unpaired high-frequency tetanic stimulation of CA2 SC inputs (Nasrallah et al., 2015; Piskorowski and Chevaleyre, 2013) or EC inputs (Nasrallah et al., 2017). Similarly, the mechanism underlying the iLTD component of ITDP in CA1 (Basu et al., 2013) resembles CB1 receptor-dependent iLTD induced by high-frequency tetanic stimulation of the CA1 SC inputs (Chevaleyre and Castillo, 2004). Thus, in both CA1 and CA2, paired low-frequency activation of the EC and SC inputs recruit similar forms of plasticity induced by high-frequency stimulation of the SC inputs alone, even though the class of inhibitory neurons mediating the plasticity in these two regions differs. This raises the interesting question as to why distinct IN populations contribute to iLTD and ITDP in neighboring hippocampal regions.

The involvement of PV⁺ INs in CA2 ITDP is consistent with findings that this region contains a higher density of PV⁺ INs compared to neighboring CA1 and CA3, both in mice (Piskorowski et al., 2016) and humans (Andrioli et al., 2007; Benes et al., 1998). Light-induced stimulation of the PV⁺ INs elicited larger IPSCs in CA2 PNs than in CA1 PNs (Piskorowski and Chevaleyre, 2013). Additionally, some PV⁺ cells in CA2 have a unique morphology and extend their dendrites and axons into all three CA subfields (Mercer et al., 2012; Mercer et al., 2007). Finally, CA2 PNs receive a much higher density of inhibitory synapses from PV⁺ INs cells compared with CA1 or CA3 (Ribak et al., 1993). These observations are consistent with the large amount of feedforward inhibition in CA2 PNs evoked by SC stimulation (Chevaleyre and Siegelbaum, 2010).

However, PV⁺ IN density alone is unlikely to account for all the differences in iLTD in CA1 compared to CA2. Thus, whereas bath application of a δ -opioid receptor agonist is sufficient to produce a long-lasting suppression of PV⁺ IN-mediated inhibition in CA2, it produces only a transient suppression of inhibition in CA1 (Piskorowski and Chevaleyre, 2013). This difference may be related to differences in δ -opioid receptor density, as radiolabeling of δ -opioid receptors was largely confined to CA2 (Duka et al., 1981), even though δ -opioid receptor mRNA expression is detected throughout the hippocampus (Erbs et al., 2012; Stumm et al., 2004).

The Site of EC and SC Input Integration and the Triggering of Enkephalin Release for the Induction of CA2 ITDP

The differential role of δ -opioid receptor-dependent plasticity in CA2 versus CA1 is also likely to depend on local differences in the release of enkephalin, the endogenous agonist for the δ -opioid receptor, as strong enkephalin radiolabeling is localized to CA2 (Sar et al., 1978). This may reflect the fact that, in the hippocampus, a major site of enkephalin release is from mossy fiber terminals, which target CA2, but not CA1 (Kohara et al., 2014). Moreover, enkephalin is also present in LEC LII stellate cells, which also target CA2, but not CA1, as well as in a sparse population of INs distributed across the different hippocampal layers (Gall et al., 1981; Simmons and Chavkin, 1996).

Despite the striking similarities between our results on CA2 ITDP and the mechanisms of iLTD, it is unclear as to whether the two protocols release enkephalin from the same cells. As 1 Hz stimulation of SC or EC inputs alone fails to elicit iLTD (97% \pm 9%, n = 5; Wilcoxon test, p = 0.1 compared to baseline for EC stimulation; see Piskorowski and Chevaleyre, 2013 for SC 1 Hz stimulation), enkephalin release appears to require strong synaptic activation. This requirement can be fulfilled either through paired stimulation of EC and SC pathways, which occurs during ITDP induction, or through high-frequency unpaired SC (Piskorowski and Chevaleyre, 2013) or EC (Nasrallah et al., 2017) stimulation. Indeed, neuropeptide release generally requires higher levels of presynaptic activity than does release of classical neurotransmitters (van den Pol, 2012). It is possible that separate populations of enkephalin-releasing neurons are differentially tuned to these forms of strong activity or that a single class of enkephalin neuron is able to respond to either pattern of input.

What is the site of integration of the EC and SC inputs during the induction of ITDP? In CA1, this integration occurs in CA1 PNs as hyperpolarization or intracellular perfusion with a Ca²⁺ chelator blocks the induction of ITDP. However, the integration of EC and SC signals during CA2 ITDP is likely to occur in a non-pyramidal neuronal or glial cell within the hippocampus because hyperpolarization of the CA2 PN population fails to inhibit ITDP. We suggest that EC and SC inputs may converge on enkephalin-expressing INs in or nearby to CA2, synergistically triggering enkephalin release.

This leads to a proposed circuit mechanism for CA2 ITDP (Figure S9). According to this model, enkephalin-expressing neurons integrate appropriately timed EC LII stellate cell and SC inputs to generate a large postsynaptic response required to release enkephalin. A large postsynaptic response can also be elicited

by strong tetanic stimulation of either pathway alone, explaining the induction of iLTD with unpaired strong EC or SC activation (Nasrallah et al., 2015, 2017; Piskorowski and Chevaleyre, 2013). As we observed ENK⁺ terminals apposed to CA2 PNs and PV soma (Figure 7), enkephalin could be released directly onto PV⁺ basket cell terminals to produce a long-lasting presynaptic inhibition of GABA release.

Physiological Relevance of ITDP in CA2 Compared to CA1

Heterosynaptic learning rules have been posited to act as salience detectors in different circuits (Basu and Siegelbaum, 2015). In CA1, ITDP has been suggested to provide a mechanism that assesses the relevance of information propagated through the trisynaptic pathway based on its temporal relation to multimodal sensory representations arriving through the direct EC inputs (Basu et al., 2013, 2016; Dudman et al., 2007). Others have shown that paired activation of EC and SC inputs to CA1 can produce shorter-term actions to boost CA1 output by promoting EPSP dendritic propagation (Jarsky et al., 2005) or burst firing of action potentials (Takahashi and Magee, 2009). A potential behavioral role of CA1 ITDP, or a related plasticity mechanism, was recently suggested by a study from our laboratory in which the long-range inhibitory inputs from EC to CA1 were inactivated using a pharmacogenetic approach (Basu et al., 2016). Silencing the long-range inhibitory inputs prevents the induction of CA1 ITDP, decreases the specificity of contextual fear memory, and reduces performance in a novel object recognition memory test.

In a similar manner to CA1 ITDP, we find that a plasticity mechanism related to CA2 ITDP and/or iLTD may also be required for optimal CA2-dependent memory performance. Thus, the infusion of the δ -opioid receptor antagonist naltrindole into CA2 was sufficient to reduce performance on a social memory task. As the δ -opioid receptor antagonist blocks both iLTD and ITDP, we cannot determine whether the impairment in social memory results from a loss of ITDP, iLTD, or some other δ -opioid receptor-dependent mechanism that targets inhibition. Nonetheless, this pharmacological result, together with our findings that social interaction with a novel animal is sufficient to reduce feedforward inhibition and occlude further induction of ITDP, strongly supports the view that ITDP, iLTD, or a closely related process plays an important role in social memory storage.

The finding that CA2 ITDP can be induced with much weaker, lower-frequency stimulation compared to CA2 iLTD suggests that ITDP is likely to be recruited preferentially under physiological conditions of sparse firing patterns observed *in vivo*, such as during the 1 Hz EC hippocampal firing frequency observed in rodents during exploratory behavior (Csicsvari et al., 1999; Frank et al., 2001). The 20 ms timing dependence of ITDP also suggests a potential physiological relevance, as this delay matches the delay in which information is propagated through the trisynaptic versus direct EC inputs during electrical stimulation *in vivo* (Yeckel and Berger, 1990), and matches the period of network-dependent gamma frequency oscillations. However, little is known about the *in vivo* dynamics of CA2 EC and SC inputs during social interactions or other behaviors. Thus, future *in vivo* monitoring of EC and SC inputs to CA2 during social memory

storage, although challenging, would help assess the potential relevance of ITDP under more physiological conditions.

What are the relative roles of the direct EC versus SC inputs to CA2 in social memory? As CA2 PNs are weakly excited by their SC inputs (as a result of strong feedforward inhibition) but are strongly excited by their direct EC inputs (Chevaleyre and Siegelbaum, 2010), the SC inputs were proposed to primarily act in CA2 to prevent information flow through a quadrisynaptic path (EC → DG → CA3 → CA2 → CA1). Our findings implicating ITDP and/or iLTD of SC-evoked feedforward inhibition to CA2 in social memory suggest that the SC inputs may provide important information for social memory storage. These observations complement the findings of a previous study linking the potentiation of the SC-evoked EPSP in CA2 PNs by vasopressin (Pagani et al., 2015) to a vasopressin-dependent enhancement in social memory (Smith et al., 2016). Optimal social memory storage may require both the δ -opioid receptor-mediated depression of SC-evoked feedforward inhibition and the vasopressin-mediated potentiation of the SC-evoked EPSP in CA2 PNs. The potentiation of the SC EPSP by vasopressin could account for the residual social memory that we observed in the presence of the δ -opioid receptor antagonist.

Our results on the importance of PV⁺ INs in CA2 social memory storage add to the growing literature of the importance of these neurons in different plasticity mechanisms that may contribute to diverse forms of hippocampal-dependent learning and memory. Thus, hippocampal PV⁺ INs have recently been linked with memory consolidation following single-trial contextual fear conditioning (Ognjanovski et al., 2017), effects of environmental enrichment, and Pavlovian contextual fear conditioning (Donato et al., 2013). Moreover, environmental enrichment and Pavlovian conditioning triggered the differentiation of the PV⁺ IN network into low-expressing and high-expressing PV⁺ configurations, respectively (Donato et al., 2013). The low-PV⁺ configuration was associated with enhanced structural synaptic plasticity and memory consolidation and retrieval, which were reduced in the high-PV configuration. Whether other forms of PV⁺ neuron plasticity also contribute to social memory storage in CA2 in addition to ITDP/iLTD remains to be determined.

Finally, recent findings that ventral CA1 is also required for social memory (Okuyama et al., 2016) suggest that plasticity in CA2 may ultimately be expressed by enhanced activation of downstream CA1 PNs. Although further studies will be important to dissect the relative contributions of different circuit elements and plasticity mechanisms to social memory storage, our results, together with previous findings from our laboratory on CA1 ITDP (Basu et al., 2016), suggest that ITDP-mediated enhancement of information flow through the SC pathway may provide a widespread synaptic learning rule that can be tuned to the local molecular and cellular circuitry to enhance performance in circuit-specific hippocampal-dependent memory tasks.

STAR★METHODS

Detailed methods are provided in the online version of this paper and include the following:

- KEY RESOURCES TABLE
- CONTACT FOR REAGENT AND RESOURCE SHARING

- **EXPERIMENTAL MODEL AND SUBJECT DETAILS**
- **METHOD DETAILS**
 - Slice Preparation
 - Electrophysiological Recordings
 - Virus Injections
 - Immunohistochemistry
 - Direct Interaction Test
 - Occlusion Experiments
- **QUANTIFICATION AND STATISTICAL ANALYSIS**
 - Data Analysis for Electrophysiology
 - Data Analysis for Behavior

SUPPLEMENTAL INFORMATION

Supplemental Information includes nine figures and two movies and can be found with this article online at <http://dx.doi.org/10.1016/j.neuron.2017.07.036>.

AUTHOR CONTRIBUTIONS

Conceptualization, F.L. and S.A.S.; Investigation, F.L., D.H.B., and T.M.; F.L. performed intra-cellular recordings; F.L. and T.M. performed the behavioral assays; F.L. and D.H.B. performed the immunohistochemistry and the viral injections; Writing – Original draft, F.L.; Writing – Review and editing, F.L. and S.A.S.; Visualization, F.L.; Supervision, S.A.S.; Funding acquisition, S.A.S.

ACKNOWLEDGMENTS

The authors thank Matt Bailey and Eleanor Simpson for their advice with the micro-perfusion system as well as Jung Park for his help preparing the videos. We are also grateful to Thomas Reardon for providing us with the N2C rabies virus and associated glycoprotein expressing rAAV. This work was supported by R01-MH104602 and R01-MH106629 from NIH (S.A.S.) and by PD/BD/113700/2015 from the Portuguese Foundation for Science and Technology (T.M.).

Received: December 15, 2016

Revised: May 26, 2017

Accepted: July 28, 2017

Published: August 17, 2017

REFERENCES

- Alger, B.E., and Teyler, T.J. (1976). Long-term and short-term plasticity in the CA1, CA3, and dentate regions of the rat hippocampal slice. *Brain Res.* *110*, 463–480.
- Andrioli, A., Alonso-Nanclares, L., Arellano, J.I., and DeFelipe, J. (2007). Quantitative analysis of parvalbumin-immunoreactive cells in the human epileptic hippocampus. *Neuroscience* *149*, 131–143.
- Basu, J., and Siegelbaum, S.A. (2015). The corticohippocampal circuit, synaptic plasticity, and memory. *Cold Spring Harb. Perspect. Biol.* *7*, 7.
- Basu, J., Srinivas, K.V., Cheung, S.K., Taniguchi, H., Huang, Z.J., and Siegelbaum, S.A. (2013). A cortico-hippocampal learning rule shapes inhibitory microcircuit activity to enhance hippocampal information flow. *Neuron* *79*, 1208–1221.
- Basu, J., Zaremba, J.D., Cheung, S.K., Hitti, F.L., Zemelman, B.V., Losonczy, A., and Siegelbaum, S.A. (2016). Gating of hippocampal activity, plasticity, and memory by entorhinal cortex long-range inhibition. *Science* *351*, aaa5694.
- Benes, F.M., Kwok, E.W., Vincent, S.L., and Todtenkopf, M.S. (1998). A reduction of nonpyramidal cells in sector CA2 of schizophrenics and manic depressives. *Biol. Psychiatry* *44*, 88–97.
- Blasco-Ibáñez, J.M., Martínez-Guijarro, F.J., and Freund, T.F. (1998). Enkephalin-containing interneurons are specialized to innervate other inter-

neurons in the hippocampal CA1 region of the rat and guinea-pig. *Eur. J. Neurosci.* *10*, 1784–1795.

Bliss, T.V., and Lomo, T. (1973). Long-lasting potentiation of synaptic transmission in the dentate area of the anaesthetized rabbit following stimulation of the perforant path. *J. Physiol.* *232*, 331–356.

Burstein, S.R., Williams, T.J., Lane, D.A., Knudsen, M.G., Pickel, V.M., McEwen, B.S., Waters, E.M., and Milner, T.A. (2013). The influences of reproductive status and acute stress on the levels of phosphorylated delta opioid receptor immunoreactivity in rat hippocampus. *Brain Res.* *1518*, 71–81.

Chavkin, C., Bakhit, C., and Bloom, F.E. (1983). Evidence for dynorphin-A as a neurotransmitter in rat hippocampus. *Life Sci.* *33 (Suppl 1)*, 13–16.

Chavkin, C., Shoemaker, W.J., McGinty, J.F., Bayon, A., and Bloom, F.E. (1985). Characterization of the prodynorphin and proenkephalin neuropeptide systems in rat hippocampus. *J. Neurosci.* *5*, 808–816.

Chevalyere, V., and Castillo, P.E. (2004). Endocannabinoid-mediated metaplasticity in the hippocampus. *Neuron* *43*, 871–881.

Chevalyere, V., and Siegelbaum, S.A. (2010). Strong CA2 pyramidal neuron synapses define a powerful disinaptic cortico-hippocampal loop. *Neuron* *66*, 560–572.

Cho, J.H., Bayazitov, I.T., Meloni, E.G., Myers, K.M., Carlezon, W.A., Jr., Zakharenko, S.S., and Bolshakov, V.Y. (2011). Coactivation of thalamic and cortical pathways induces input timing-dependent plasticity in amygdala. *Nat. Neurosci.* *15*, 113–122.

Chow, B.Y., Han, X., Dobry, A.S., Qian, X., Chuong, A.S., Li, M., Henninger, M.A., Belfort, G.M., Lin, Y., Monahan, P.E., and Boyden, E.S. (2010). High-performance genetically targetable optical neural silencing by light-driven proton pumps. *Nature* *463*, 98–102.

Commons, K.G., and Milner, T.A. (1996). Ultrastructural relationships between leu-enkephalin- and GABA-containing neurons differ within the hippocampal formation. *Brain Res.* *724*, 1–15.

Csicsvari, J., Hirase, H., Czurkó, A., Mamiya, A., and Buzsáki, G. (1999). Oscillatory coupling of hippocampal pyramidal cells and interneurons in the behaving Rat. *J. Neurosci.* *19*, 274–287.

Donato, F., Rompani, S.B., and Caroni, P. (2013). Parvalbumin-expressing basket-cell network plasticity induced by experience regulates adult learning. *Nature* *504*, 272–276.

Dudek, S.M., Alexander, G.M., and Farris, S. (2016). Rediscovering area CA2: unique properties and functions. *Nat. Rev. Neurosci.* *17*, 89–102.

Dudman, J.T., Tsay, D., and Siegelbaum, S.A. (2007). A role for synaptic inputs at distal dendrites: instructive signals for hippocampal long-term plasticity. *Neuron* *56*, 866–879.

Duka, T., Wüster, M., Schubert, P., Stoiber, R., and Herz, A. (1981). Selective localization of different types of opiate receptors in hippocampus as revealed by in vitro autoradiography. *Brain Res.* *205*, 181–186.

Erbs, E., Faget, L., Scherrer, G., Kessler, P., Hentsch, D., Vonesch, J.L., Matifas, A., Kieffer, B.L., and Massotte, D. (2012). Distribution of delta opioid receptor-expressing neurons in the mouse hippocampus. *Neuroscience* *221*, 203–213.

Frank, L.M., Brown, E.N., and Wilson, M.A. (2001). A comparison of the firing properties of putative excitatory and inhibitory neurons from CA1 and the entorhinal cortex. *J. Neurophysiol.* *86*, 2029–2040.

Fuentealba, P., Tomioka, R., Dalezios, Y., Márton, L.F., Studer, M., Rockland, K., Klausberger, T., and Somogyi, P. (2008). Rhythmically active enkephalin-expressing GABAergic cells in the CA1 area of the hippocampus project to the subiculum and preferentially innervate interneurons. *J. Neurosci.* *28*, 10017–10022.

Gall, C., Brecha, N., Karten, H.J., and Chang, K.J. (1981). Localization of enkephalin-like immunoreactivity to identified axonal and neuronal populations of the rat hippocampus. *J. Comp. Neurol.* *198*, 335–350.

Hippenmeyer, S., Vrieseling, E., Sigrist, M., Portmann, T., Laengle, C., Ladle, D.R., and Arber, S. (2005). A developmental switch in the response of DRG neurons to ETS transcription factor signaling. *PLoS Biol.* *3*, e159.

- Hitti, F.L., and Siegelbaum, S.A. (2014). The hippocampal CA2 region is essential for social memory. *Nature* 508, 88–92.
- Ito, M. (2001). Cerebellar long-term depression: characterization, signal transduction, and functional roles. *Physiol. Rev.* 81, 1143–1195.
- Jarsky, T., Roxin, A., Kath, W.L., and Spruston, N. (2005). Conditional dendritic spike propagation following distal synaptic activation of hippocampal CA1 pyramidal neurons. *Nat. Neurosci.* 8, 1667–1676.
- Junyent, F., and Kremer, E.J. (2015). CAV-2—why a canine virus is a neurobiologist's best friend. *Curr. Opin. Pharmacol.* 24, 86–93.
- Kitamura, T., Pignatelli, M., Suh, J., Kohara, K., Yoshiki, A., Abe, K., and Tonegawa, S. (2014). Island cells control temporal association memory. *Science* 343, 896–901.
- Kogan, J.H., Frankland, P.W., and Silva, A.J. (2000). Long-term memory underlying hippocampus-dependent social recognition in mice. *Hippocampus* 10, 47–56.
- Kohara, K., Pignatelli, M., Rivest, A.J., Jung, H.Y., Kitamura, T., Suh, J., Frank, D., Kajikawa, K., Mise, N., Obata, Y., et al. (2014). Cell type-specific genetic and optogenetic tools reveal hippocampal CA2 circuits. *Nat. Neurosci.* 17, 269–279.
- Kowalski, J., Gan, J., Jonas, P., and Pernia-Andrade, A.J. (2016). Intrinsic membrane properties determine hippocampal differential firing pattern in vivo in anesthetized rats. *Hippocampus* 26, 668–682.
- McGinty, J.F., Henriksen, S.J., Goldstein, A., Terenius, L., and Bloom, F.E. (1983). Dynorphin is contained within hippocampal mossy fibers: immunohistochemical alterations after kainic acid administration and colchicine-induced neurotoxicity. *Proc. Natl. Acad. Sci. USA* 80, 589–593.
- Mercer, A., Trigg, H.L., and Thomson, A.M. (2007). Characterization of neurons in the CA2 subfield of the adult rat hippocampus. *J. Neurosci.* 27, 7329–7338.
- Mercer, A., Botcher, N.A., Eastlake, K., and Thomson, A.M. (2012). SP-SR interneurons: a novel class of neurons of the CA2 region of the hippocampus. *Hippocampus* 22, 1758–1769.
- Nasrallah, K., Piskorowski, R.A., and Chevaleyre, V. (2015). Inhibitory plasticity permits the recruitment of CA2 pyramidal neurons by CA3(1,2,3). *eNeuro* 2, ENEURO.0049-15.2015.
- Nasrallah, K., Piskorowski, R.A., and Chevaleyre, V. (2017). Bi-directional interplay between proximal and distal inputs to CA2 pyramidal neurons. *Neurobiol. Learn. Mem.* 138, 173–181.
- Ognjanovski, N., Schaeffer, S., Wu, J., Mofakham, S., Maruyama, D., Zochowski, M., and Aton, S.J. (2017). Parvalbumin-expressing interneurons coordinate hippocampal network dynamics required for memory consolidation. *Nat. Commun.* 8, 15039.
- Okuyama, T., Kitamura, T., Roy, D.S., Itohara, S., and Tonegawa, S. (2016). Ventral CA1 neurons store social memory. *Science* 353, 1536–1541.
- Pagani, J.H., Zhao, M., Cui, Z., Avram, S.K., Caruana, D.A., Dudek, S.M., and Young, W.S. (2015). Role of the vasopressin 1b receptor in rodent aggressive behavior and synaptic plasticity in hippocampal area CA2. *Mol. Psychiatry* 20, 490–499.
- Piskorowski, R.A., and Chevaleyre, V. (2013). Delta-opioid receptors mediate unique plasticity onto parvalbumin-expressing interneurons in area CA2 of the hippocampus. *J. Neurosci.* 33, 14567–14578.
- Piskorowski, R.A., Nasrallah, K., Diamantopoulou, A., Mukai, J., Hassan, S.I., Siegelbaum, S.A., Gogos, J.A., and Chevaleyre, V. (2016). Age-dependent specific changes in area CA2 of the hippocampus and social memory deficit in a mouse model of the 22q11.2 deletion syndrome. *Neuron* 89, 163–176.
- Reardon, T.R., Murray, A.J., Turi, G.F., Wirblich, C., Croce, K.R., Schnell, M.J., Jessell, T.M., and Losonczy, A. (2016). Rabies virus CVS-N2c(Δ G) strain enhances retrograde synaptic transfer and neuronal viability. *Neuron* 89, 711–724.
- Ribak, C.E., Seress, L., and Leranth, C. (1993). Electron microscopic immunocytochemical study of the distribution of parvalbumin-containing neurons and axon terminals in the primate dentate gyrus and Ammon's horn. *J. Comp. Neurol.* 327, 298–321.
- Safo, P., and Regehr, W.G. (2008). Timing dependence of the induction of cerebellar LTD. *Neuropharmacology* 54, 213–218.
- Sar, M., Stumpf, W.E., Miller, R.J., Chang, K.J., and Cuatrecasas, P. (1978). Immunohistochemical localization of enkephalin in rat brain and spinal cord. *J. Comp. Neurol.* 182, 17–37.
- Simmons, M.L., and Chavkin, C. (1996). Endogenous opioid regulation of hippocampal function. *Int. Rev. Neurobiol.* 39, 145–196.
- Smith, A.S., Williams Avram, S.K., Cymerblit-Sabba, A., Song, J., and Young, W.S. (2016). Targeted activation of the hippocampal CA2 area strongly enhances social memory. *Mol. Psychiatry* 21, 1137–1144.
- Stevenson, E.L., and Caldwell, H.K. (2014). Lesions to the CA2 region of the hippocampus impair social memory in mice. *Eur. J. Neurosci.* 40, 3294–3301.
- Stumm, R.K., Zhou, C., Schulz, S., and Höllt, V. (2004). Neuronal types expressing mu- and delta-opioid receptor mRNA in the rat hippocampal formation. *J. Comp. Neurol.* 469, 107–118.
- Svoboda, K.R., Adams, C.E., and Lupica, C.R. (1999). Opioid receptor subtype expression defines morphologically distinct classes of hippocampal interneurons. *J. Neurosci.* 19, 85–95.
- Takahashi, H., and Magee, J.C. (2009). Pathway interactions and synaptic plasticity in the dendritic tuft regions of CA1 pyramidal neurons. *Neuron* 62, 102–111.
- Terrian, D.M., Johnston, D., Claiborne, B.J., Ansah-Yiadom, R., Strittmatter, W.J., and Rea, M.A. (1988). Glutamate and dynorphin release from a subcellular fraction enriched in hippocampal mossy fiber synaptosomes. *Brain Res. Bull.* 21, 343–351.
- Urban, D.J., and Roth, B.L. (2015). DREADDs (designer receptors exclusively activated by designer drugs): chemogenetic tools with therapeutic utility. *Annu. Rev. Pharmacol. Toxicol.* 55, 399–417.
- van den Pol, A.N. (2012). Neuropeptide transmission in brain circuits. *Neuron* 76, 98–115.
- Wall, N.R., Wickersham, I.R., Cetin, A., De La Parra, M., and Callaway, E.M. (2010). Monosynaptic circuit tracing in vivo through Cre-dependent targeting and complementation of modified rabies virus. *Proc. Natl. Acad. Sci. USA* 107, 21848–21853.
- Xu, J.Y., Zhang, J., and Chen, C. (2012). Long-lasting potentiation of hippocampal synaptic transmission by direct cortical input is mediated via endocannabinoids. *J. Physiol.* 590, 2305–2315.
- Yeckel, M.F., and Berger, T.W. (1990). Feedforward excitation of the hippocampus by afferents from the entorhinal cortex: redefinition of the role of the trisynaptic pathway. *Proc. Natl. Acad. Sci. USA* 87, 5832–5836.

STAR★METHODS

KEY RESOURCES TABLE

REAGENT or RESOURCE	SOURCE	IDENTIFIER
Antibodies		
Met/Leu-enkephalin(NOC1/35) antibody	Santa Cruz Biotechnologies	Cat# sc-47705; RRID: AB_2161515
Leu Enkephalin antibody	Fitzgerald Industries International	Cat# 10-L20A; RRID: AB_1287677
RGS14 antibody	UC Davis/NIH NeuroMab Facility	Cat# 73-170; RRID: AB_10698026
Mouse Anti-STEP Monoclonal Antibody, Unconjugated, Clone 23E5	Cell Signaling Technology	Cat# 4396S; RRID: AB_1904101
Anti-PCP4 Antibody produced in rabbit	Sigma-Aldrich	Cat# HPA005792; RRID: AB_1855086
Chicken anti-GFP Antibody	AVES Labs	Cat# GFP-1020; RRID: AB_10000240
Reelin/CR-50 Monoclonal Antibody	MBL International	Cat# D223-3; RRID: AB_843523
Calbindin-1 Antibody	Abcam	Cat# ab11426; RRID: AB_298031
Rabbit Anti-Parvalbumin Polyclonal Antibody	Abcam	Cat# ab11427; RRID: AB_298032
Monoclonal Anti-Parvalbumin antibody produced in mouse	Sigma-Aldrich	Cat# P3088; RRID: AB_477329
CaMKII antibody [6G9]	Abcam	Cat# ab22609; RRID: AB_447192
Anti-GAD67, clone 1G10.2 antibody	Millipore	Cat# MAB5406; RRID: AB_2278725
Anti-Opioid Receptor Antibody, δ	EMD Millipore	Cat# AB1560; RRID: AB_90778
Streptavidin, Alexa 555 conjugate antibody	Thermo Fisher Scientific	Cat# s21381; RRID: AB_2307336
Goat anti-Mouse IgG (H+L) Secondary Antibody, Alexa 488 conjugate	Thermo Fisher Scientific	Cat# A11001; RRID: AB_2534069
Goat anti-Mouse IgG1 Secondary Antibody, Alexa 488 conjugate	Thermo Fisher Scientific	Cat# A21121; RRID: AB_141514
Goat anti-Mouse IgG1 Secondary Antibody, Alexa 546 conjugate	Thermo Fisher Scientific	Cat# A21123; RRID: AB_2535765
Goat anti-Mouse IgG1 Secondary Antibody, Alexa 633 conjugate	Thermo Fisher Scientific	Cat# A21126; RRID: AB_2535768
Goat anti-Mouse IgG2a Secondary Antibody, Alexa 488 conjugate	Thermo Fisher Scientific	Cat# A21131; RRID: AB_2535771
Goat anti-Mouse IgG2a Secondary Antibody, Alexa 647 conjugate	Thermo Fisher Scientific	Cat# A21241; RRID: AB_2535810
Goat anti-Rabbit IgG (H+L) Secondary Antibody, Alexa 488 conjugate	Thermo Fisher Scientific	Cat# A11008; RRID: AB_143165
Goat anti-Rabbit IgG (H+L) Secondary Antibody, Alexa 633 conjugate	Thermo Fisher Scientific	Cat# A21070; RRID: AB_2535731
Goat Anti-Chicken IgG (H+L) Secondary Antibody, Alexa 488 Conjugate	Thermo Fisher Scientific	Cat# A11039; RRID: AB_142924
Chemicals, Peptides, and Recombinant Proteins		
Naltrindole	Sigma-Aldrich	Cat# N115
ICI 174,864	Tocris	Cat# 0820
miniRuby	Thermo Fisher Scientific	Cat# D3312
AM251	Tocris	Cat# 1117
D-AP5	Tocris	Cat# 0106
CGP 55845	Tocris	Cat# 1248
SR 95531	Tocris	Cat# 1262
BAPTA	Tocris	Cat# 2786
Experimental Models: Organisms/Strains		
B6.Cg-Gt(ROSA) ^{26Sor} ^{tm1.4(CAG-tdTomato)Hze} /J Mus musculus	The Jackson Laboratory	RRID: IMSR_JAX:007914
B6.129P2-Pvalb ^{tm1(cre)Arbr} /J Mus musculus	The Jackson Laboratory	RRID: IMSR_JAX:017320
B6.Cg-Tg(Amigo2-cre)1Sieg/J Mus musculus	The Jackson Laboratory	RRID: IMSR_JAX:030215

(Continued on next page)

Continued

REAGENT or RESOURCE	SOURCE	IDENTIFIER
Recombinant DNA		
rAAV5 EF1a.DIO.hChr2(E123T/T159C).eYFP	UNC Vector Core	Addgene Cat# 35509
CAV2-cre	IGGM Viral Vector Core	N/A
rAAV2 hsyn.DIO.HA-hM4D(Gi).IRES.mCitrine	UNC Vector Core	Addgene Cat# 50455
rAAV9 CBA.FLEX.Arch3.0-GFP.WPRE.SV40	UPenn	cat#AV-5-PV2432
rAAV5 EF1a.FLEX.TVA-mCherry	UNC Vector Core	Addgene Cat# 38044
RABV ^{ΔG} -eGFP[EnvA]	Salk Institute	Addgene Cat# 32636
rAAV-FLEX-nGFP-2A-G	Thomas Reardon	Addgene Cat# 73476
RABV ^{ΔG} -mCherry[EnvA]	Thomas Reardon	Addgene Cat# 73464
rAAV9 CaMKIIa.hChr2(H134R)-EYFP	UNC Vector Core	Addgene Cat# 26969
rAAV9 CamKII.hChr2(T/C).p2A.mCherry	Stanford Vector Core	N/A
Software and Algorithms		
AxoGraph	AxoGraph	1.6.4
PRISM 7	GraphPad	7.0c
Microsoft Office Word	Microsoft	2016
Microsoft Office Excel	Microsoft	2016
Adobe Illustrator Photoshop	Adobe	CS6
Adobe Illustrator Illustrator	Adobe	CS6 16.0.4
FIJI	N/A	N/A

CONTACT FOR REAGENT AND RESOURCE SHARING

Further information and requests for reagents may be directed to, and will be fulfilled by the Lead Contact, Dr. Steven A. Siegelbaum (sas8@columbia.edu).

EXPERIMENTAL MODEL AND SUBJECT DETAILS

All animal procedures were performed in accordance with the regulations of the Columbia University IACUC. 6- to 12-week-old C57BL6/J male mice were used in this study for most electrophysiological and labeling studies. When required, we also used males of the same age range from the following transgenic mouse lines PV-Cre mice (Jackson Laboratories #017320), Ai14 mice (Jackson Laboratories #007914) and Amigo2-cre (Jackson Laboratories #030215). Noteworthy, all transgenic mice used in this study were kept on a C57BL6/J strain background.

METHOD DETAILS**Slice Preparation**

We prepared transverse hippocampal slices from 8- to 12-week-old C57BL6 male mice. Animals were killed under isoflurane anesthesia by perfusion into the right ventricle of ice-cold solution containing the following (in mM): 10 NaCl, 195 sucrose, 2.5 KCl, 10 glucose, 25 NaHCO₃, 1.25 NaH₂PO₄, 7 Na Pyruvate, 1.25 CaCl₂, and 0.5 MgCl₂. Hippocampi were dissected from the brain in the same dissecting solution, placed upright into a 4% agar mold, and cut into 400 μm slices with a vibratome (VT1200S, Leica) in the same ice-cold dissection solution. Slices were then transferred to a chamber containing 50% dissecting solution and 50% ACSF (in mM: 125 NaCl, 2.5 KCl, 22.5 glucose, 25 NaHCO₃, 1.25 NaH₂PO₄, 3 Na Pyruvate, 1 Ascorbic acid, 2 CaCl₂ and 1 MgCl₂). The chamber was kept at 34°C for 30 min and then at room temperature for at least 1 h before recording. All experiments were performed at 33°C. Dissecting and recording solutions were both saturated with 95% O₂ and 5% CO₂, pH 7.4.

Electrophysiological Recordings

Slices were mounted in the recording chamber under a microscope. Recordings were acquired using the Multiclamp 700A amplifier (Molecular Device), data acquisition interface ITC-18 (Instrutech) and the Axograph X software.

We targeted CA2 PNs based on somatic location and size in both deep and superficial layer. Whole-cell recordings were obtained from CA2 PNs in current-clamp mode with a patch pipette (3–5 MΩ) containing the following (in mM): 135 K methylsulfate, 5 KCl, 0.2 EGTA-Na, 10 HEPES, 2 NaCl, 5 ATP, 0.4 GTP, 10 phosphocreatine, and 5 μM biocytin, pH 7.2 (280–290 mOsm). Liquid junction

potential was 1.2 mV and was left uncorrected. Inhibitory currents were recorded with pipette solution containing 135 Cs methylsulfate instead of K methylsulfate. Series resistance (15–25 M Ω) was monitored throughout each experiment; cells with a > 20% change in series resistance were discarded. Once whole-cell recording was achieved we confirmed the cell-type based on the following electrophysiological properties: input resistance (60 to 120 M Ω), resting membrane potential (below –70 mV), sag amplitude (smaller than 5 mV) and presence of a slow depolarization prior discharge upon the injection of a long current pulse (Figure 1A1).

For electrical stimulation, synaptic potentials from the Schaffer collateral (SC) and entorhinal cortex fibers (EC) were evoked by monopolar stimulation with pipettes filled with 1M NaCl and positioned in the *stratum radiatum* (SR) of CA3 (SC stimulation) as well as in the *stratum lacunosum-moleculare* (SLM) of CA1c, near the hippocampal fissure (EC stimulation, Figure 1B1). The ITDP induction protocol (90 paired pulses at 1 Hz with EC stimulation 20 ms prior to the SC stimulation, Dudman et al., 2007) was applied after a stable baseline of 5 min at least 10 min following breaking into the cell.

For light stimulation, pulses of blue or yellow light (pE-100, Cool LED) were delivered through a 40x immersion objective and illuminated an area of 0.2 mm². The illumination field was centered over the CA2 pyramidal cell layer for yellow light illumination and over the SLM layer for blue light illumination.

In a subset of experiments, the following drugs were used at the following concentrations via bath application: SR95531 (2 mM, Tocris #1262), CGP55845 (1 mM, Tocris #1248), AM251 (2 mM, Tocris #1117), D-APV (100 mM, Tocris #0106), ICI 174,864 (2 μ M, Tocris #0820), BAPTA (20 mM, Tocris #2786) and naltrindole (0.1 μ M, Sigma-Aldrich #N115).

Virus Injections

For all injections, animals were anesthetized using isoflurane and given analgesics. A craniotomy was performed above the target region and a glass pipette was stereotaxically lowered down to the desired depth. Injections were performed using a nano-inject II (Drummond Scientific company). 23 nL was delivered 15 s apart until total amount was reached. The pipette was retracted after 5 min.

iDREADD and Arch3.0 Hippocampal Injections

We injected bilaterally 200 nL of either rAAV2 hsyn.DIO.HA-hM4D(Gi).IRES.mCitrine (Addgene #50455 prepared by the UNC vector core) or rAAV9 CBA.FLEX.Arch3.0-GFP.WPRE.SV40 (U Penn, AV-5-PV2432, lot V42-43MI-S, prepared from Addgene #22222) into the hippocampi of PV-Cre mice (Jackson Laboratories #017320) or Amigo2-cre mice (Jackson Laboratories #030215). Injection coordinates were the following (in mm from Bregma): AP 1.6, ML \pm 1.6, DV 1.7. Acute slices were prepared 3 weeks after the injection.

Rabies Tracing

We injected bilaterally 50 nL of a 1:2 cocktail of rAAV5 EF1a.FLEX.TVA-mCherry (Addgene #38044 prepared by UNC vector core) with rAAV5 CAG.FLEX.RAB[G] (Addgene #48333 prepared by UNC vector core) into the dorsal hippocampus of Amigo2-cre mouse (Hitti and Siegelbaum, 2014): AP 1.6, ML \pm 1.6, DV 1.7 (in mm from Bregma). Following 2 weeks of recovery and rAAV expression, a secondary surgery was performed by the same technique and 300 nL of RABV Δ G-eGFP[EnvA] (SAD-B19 strain, Addgene #32636 prepared by the Salk institute vector core) was injected at the same coordinates. Mice were killed 7 d later and the brains cut sagittally for EC imaging or coronally for HC imaging. We repeated these experiments using 50 nL of the helper viruses rAAV5 EF1a.FLEX.TVA-mCherry mixed with rAAV-FLEX-nGFP-2A-G (histone2B-GFP fusion: nGFP, Addgene # 73476; Reardon et al., 2016) and followed by 300 nL of the rabies virus RABV Δ G-mCherry[EnvA] (CVS-N2c strain, Addgene #73464; Reardon et al., 2016).

Channelrhodopsin Expression into the MEC

We injected 200 nL of rAAV9 CaMKIIa.hChR2(H134R)-EYFP (Addgene #26969 prepared by UNC vector core) into the MEC at the following coordinates: AP –4.7, ML \pm 3.35 and DV –3.3 (in mm from Bregma). Animals were processed for acute slice physiology 10–15 days after. Because of the extensive overlapping of GFP⁺ fibers in the EC we used a similar virus expressing cell-filling diffusible mCherry to check for the specificity of the expression. To label the somas, we injected 200 nL of rAAV9 CamKII.hChR2(T/C).p2A.mCherry (prepared by Stanford vector core) at the same coordinates and perfused the mice after 15 days.

Dual Viral Injections to Target the EC LII Stellate Cells

We injected bilaterally 50 nL of CAV2-Cre virus (molecular genetic institute of Montpellier viral vector core, Junyent and Kremer, 2015) into the DG of Ai14 mice (Jackson Laboratories #007914). Animals were perfused 10 days later and sagittal slices were prepared to visualize the LEC. We repeated these injections on WT animals followed 10 days later by the bilateral injection of 200 nL rAAV5 EF1a.DIO.hChR2(E123T/T159C).eYFP (Addgene #35509 prepared by the UNC vector core, lot AV4828b) into the LEC. Acute slices were prepared from the animals 10–15 days later.

Immunohistochemistry

Mice were intra-cardiacly perfused using saline then 4% PFA in PBS. The brains were quickly extracted and incubated in 4% PFA overnight. After 1 h washing in 0.3% glycine in PBS, 60 μ m slices were prepared (Leica VT1000S). After fixation, slices were permeabilised and blocked for 2h with 5% goat-serum and 0.5% Triton-X in PBS. Slices were incubated overnight with primary antibodies at 4°C diluted in 5% goat-serum and 0.1% Triton-X in PBS. The slices were washed 3 times 15 min in PBS and secondary antibodies were applied at room temperature for 2 h at a concentration of 1:500 in 5% goat-serum and 0.2% Triton-X in PBS. For post hoc immunocytochemistry after patch-clamp recordings, slices were fixed for 1 h in 4% PFA in PBS and streptavidin-Alexa 555 (1:500, Thermo Fisher Scientific, Cat# s21381) was applied during primary and secondary incubations. All secondary antibodies were

produced in the goat. DAPI staining was performed (Hoechst 33342 at 1:1000 for 5 min in PBS at RT) prior to mounting the slice using fluoromount (Sigma-Aldrich). Images were acquired using an inverted confocal microscope (Leica LSM 700).

For STEP and biocytin staining, first incubation was performed with primary antibody mouse isotype1 antibody to STEP (1:500, Cell Signaling Technology, Cat# 4396S) as well as streptavidin conjugated to Alexa 555 (1:500, Thermo Fisher Scientific, Cat# s21381). Secondary incubation was performed in the presence of the antibody to mouse isotype 1 conjugated to Alexa 488 (1:500, 1:500, Thermo Fisher Scientific, Cat# A21121) as well as streptavidin conjugated to Alexa 555 (1:500, Thermo Fisher Scientific, Cat# s21381).

For δ -opioid receptor and PV staining, first incubation was performed with a mouse antibody to PV (1:4000, Sigma-Aldrich, Cat# P3088) and rabbit antibody to δ -opioid receptor (1:250, EMD Millipore, Cat# AB1560). They were followed by the secondary antibody to rabbit conjugated to Alexa 488 (1:500, Thermo Fisher Scientific, Cat# A11008) and the secondary antibody to mouse IgG1 conjugated to Alexa 633 (1:500, Thermo Fisher Scientific, Cat# A21126).

For mCitrine and RGS 14 staining, first incubation was performed with a chicken antibody to GFP (1:1000, AVES Labs, Cat# GFP-1020) and mouse antibody to RGS14 (1:50, UC Davis/NIH NeuroMab Facility, Cat# 73-170). They were followed by the secondary antibody to chicken conjugated to Alexa 488 (1:500, Thermo Fisher Scientific, Cat# A11039) and the secondary antibody to mouse IgG2a conjugated to Alexa 647 (1:500, Thermo Fisher Scientific, Cat# A21241).

For Parvalbumin and mCitrine staining, first incubation was performed with the following primary antibodies: rabbit antibody to parvalbumin (1:500, Abcam, Cat# ab11427) and chicken antibody to GFP (1:1000, AVES Labs, Cat# GFP-1020). Secondary incubation was performed with the following: antibody to rabbit conjugated to Alexa 633 (1:500, Thermo Fisher Scientific, Cat# A21070) and antibody to chicken conjugated to Alexa 488 (1:500, Thermo Fisher Scientific, Cat# A11039).

For mCitrine and biocytin staining, first incubation was performed with the following: chicken antibody to GFP (1:1000, AVES Labs, Cat# GFP-1020) and streptavidin conjugated to Alexa 555 (1:500, Thermo Fisher Scientific, Cat# s21381). Secondary incubation was performed with the following: antibody to chicken conjugated to Alexa 488 (1:500, Thermo Fisher Scientific, Cat# A11039) and streptavidin conjugated to Alexa 555 (1:500, Thermo Fisher Scientific, Cat# s21381).

For YFP, biocytin and PCP4 staining, first incubation was performed with the following: chicken antibody anti-GFP (1:1000, AVES Labs, Cat# GFP-1020), rabbit antibody to PCP4 (1:200, Sigma-Aldrich, Cat# HPA005792) and streptavidin conjugated to Alexa 555 (1:500, Thermo Fisher Scientific, Cat# s21381). Secondary incubation was performed with the following: antibody to chicken conjugated to Alexa 488 (1:500, Thermo Fisher Scientific, Cat# A11039), streptavidin conjugated to Alexa 555 (1:500, Thermo Fisher Scientific, Cat# s21381) and antibody to rabbit conjugated to Alexa 633 (1:500, Thermo Fisher Scientific, Cat# A21070).

For YFP, reelin and calbindin 1 staining, first incubation was performed with the following: chicken antibody to GFP (1:1000, AVES Labs, Cat# GFP-1020), mouse antibody to reelin (1:250, MBL International, Cat# D223-3) and rabbit antibody to calbindin1 (1:1000, Abcam, Cat# ab11426). Secondary incubation was performed with the following: antibody to chicken conjugated to Alexa 488 (1:500, Thermo Fisher Scientific, Cat# A11039), antibody to mouse IgG1 conjugated to Alexa 546 (1:250, Thermo Fisher Scientific, Cat# A21123) and antibody to rabbit conjugated to Alexa 633 (1:500, Thermo Fisher Scientific, Cat# A21070).

For YFP, biocytin and RGS14 staining, first incubation was performed with the following: chicken antibody to GFP (1:1000, AVES Labs, Cat# GFP-1020), streptavidin conjugated to Alexa 555 (1:500, S21381, Thermo Fisher) and mouse IgG2a antibody to RGS14 (1:50, UC Davis/NIH NeuroMab Facility, Cat# 73-170). Secondary incubation was performed with the following: antibody to chicken conjugated to Alexa 488 (1:500, Thermo Fisher Scientific, Cat# A11039), streptavidin conjugated to Alexa 555 (1:500, Thermo Fisher Scientific, Cat# s21381) and antibody to mouse IgG2a conjugated to Alexa 647 (1:500, Thermo Fisher Scientific, Cat# A21241).

For enkephalin and parvalbumin staining, first incubation was performed with the following: mouse antibody to enkephalin (1:50, Fitzgerald Industries International, Cat# 10-L20A; [Figures 7A and 7B](#) or 1:50, Santa Cruz Biotechnologies, Cat# sc-47705; [Figure 7C](#)) as well as rabbit antibody to parvalbumin (1:500, Abcam, Cat# ab11427). Secondary incubation was performed with the following: antibody to mouse conjugated to Alexa 488 (1:500, Thermo Fisher Scientific, Cat# A11001) and antibody to rabbit conjugated to Alexa 633 (1:500, Thermo Fisher Scientific, Cat# A21070).

For TdTomato, CaMKII and GAD67 staining, first incubation was performed with the following: mouse antibody to GAD67 (1:1000, Millipore, Cat# MAB5406) and rabbit antibody to CaMKII (1:200, Abcam, Cat# ab22609). We did not stain for TdTomato since the endogenous fluorescent signal was bright enough. Secondary incubation was performed with the following: antibody to mouse IgG2a conjugated to Alexa 488 (1:500, Thermo Fisher Scientific, Cat# A21131) and antibody to rabbit conjugated to Alexa 633 (1:500, Thermo Fisher Scientific, Cat# A21070).

For TdTomato, reelin and calbindin1 staining, first incubation was performed with the following: mouse antibody to reelin (1:250, MBL International, Cat# D223-3) and rabbit antibody to calbindin 1 (1:1000, Abcam, Cat# ab11426). We did not stain for TdTomato since the endogenous fluorescent signal was bright enough. Secondary incubation was performed with the following: antibody to mouse IgG1 conjugated to Alexa 633 (1:500, Thermo Fisher Scientific, Cat# A21126) and antibody to rabbit conjugated to Alexa 488 (1:500, Thermo Fisher Scientific, Cat# A11008).

For mCherry and reelin staining, first incubation was performed with a mouse antibody to reelin (1:250, MBL International, Cat# D223-3) followed by the secondary antibody to mouse IgG1 conjugated to Alexa 633 (1:500, Thermo Fisher Scientific, Cat# A21126). We did not stain for mCherry since the endogenous fluorescent signal was bright enough.

Direct Interaction Test

For social recognition experiments we used 3-month-old grouped house mice (5 per cages). Mice were implanted with a cannula guide extending for 1.5 mm (C315G 2-G11-SPC, Plastics One). The scalp was removed and scored before holes were drilled (AP -2 mm; ML ± 3 mm from Bregma). Cannula guides were implanted bilaterally at a 10° angle and kept in place using glue. The skull was then covered with dental cement (GC FujiCEM 2) and dummy cannulas (C315DC-SPC, Plastics One) were inserted into the guides. Mice were returned to their home cage and left to recover for 1 week.

For the direct interaction test we used the procedure described by [Kogan et al. \(2000\)](#) adapted to accommodate the micro-infusion. The procedure was performed shortly after the beginning of the dark cycle. Mice were placed under a light isoflurane anesthesia (2%) and the dummy cannulas were removed. We inserted cannulas projecting 0.5 mm from the cannula guide (C315I-SPC, Plastics One) and screwed them onto the guides. $1 \mu\text{L}$ of $5 \mu\text{M}$ naltrindole diluted in 0.9% saline or $1 \mu\text{L}$ of 0.9% saline was injected on each side over 10 min using a syringe pusher (Fusion 200, Chemix Inc.) mounted with two $2 \mu\text{L}$ syringes (88511, Hamilton). Cannulas were removed 2 min after the end of the micro-infusion to avoid pulling out the drug when removing the cannulas. Mice typically recovered fully from the light anesthesia within 5 min.

At the end of the infusion, mice were single-housed into plastic boxes of dimensions similar to their home cage (length $13''$ length x $7\text{-}1/2''$ width) but taller ($8\text{-}1/4''$ height) to allow filming the interactions from the top (see [Movies S1](#) and [S2](#)) while preventing them from escaping. Boxes contained fresh litter. Mice were left to habituate for 30 min in the behavioral room under dim light conditions. A grouped-housed male juvenile mouse (4-week old) was then placed in each box for a first interaction trial of 2 min. Following a 30 min inter-trial delay, the same juvenile was placed into the adult's cage for a second 2 min test trial. Mice were then returned to their respective home cages.

Occlusion Experiments

10-week old WT male mice were left to habituate for 30 min in a clean cage before being exposed to a 4-week old juvenile for 2 min. The juvenile was removed and the animal sacrificed 30 min later. Slices were prepared as indicated above. In order to measure the baseline CA2 feedforward inhibition we repeated the experiment described above and exposed the recorded mouse either to a novel juvenile or to a littermate for 2 min.

QUANTIFICATION AND STATISTICAL ANALYSIS

Data Analysis for Electrophysiology

The amplitudes of the PSPs were normalized to the baseline. The magnitude of plasticity was estimated by comparing averaged responses at 30–35 min after the induction protocol with baseline-averaged responses 0–10 min before the induction protocol. All drugs were bath-applied following dilution into the external solution from stock solutions. We used Axograph X software for data acquisition, and Excel (Microsoft) and PRISM (Graphpad) for data analysis. Wilcoxon or Mann-Whitney tests were performed with PRISM for statistical comparisons of paired or non-paired data respectively. Unless stated otherwise, *p* values come from Mann-Whitney tests. Results presented in the text and figures are reported as the mean \pm SEM. * is for $p < 0.05$, ** is for $p < 0.01$ and *** is for $p < 0.001$.

Data Analysis for Behavior

2-min films were scored offline for social interaction by a trained observer blind to the experimental condition. Sniffing of any part of the body, allogrooming and close following (within 1 cm) of the juvenile counted as social interaction (see on the top right corner of the video when the mention “social” appears). Adults were required to investigate the juveniles for a minimum of 24 s during the initial trial. One mouse did not meet this criterion and was excluded from the analysis. We observed no aggression. Percentage of decline was calculated by dividing the time a mouse interacted during the second trial by the time it interacted during the first trial. Wilcoxon or Mann-Whitney tests were performed with PRISM for statistical comparisons of paired or non-paired data respectively. Results presented in the text and figures are reported as the mean \pm SEM. * is for $p < 0.05$, ** is for $p < 0.01$ and *** is for $p < 0.001$.

Update

Neuron

Volume 102, Issue 1, 3 April 2019, Page 260–262

DOI: <https://doi.org/10.1016/j.neuron.2019.03.021>

Input-Timing-Dependent Plasticity in the Hippocampal CA2 Region and Its Potential Role in Social Memory

Felix Leroy,* David H. Brann, Torcato Meira, and Steven A. Siegelbaum*

*Correspondence: felxfel@aol.com (F.L.), sas8@columbia.edu (S.A.S.)

<https://doi.org/10.1016/j.neuron.2019.03.021>

(Neuron 95, 1089–1102.e1–e5; August 30, 2017)

In the original publication of this paper, we reported that paired activation of the direct cortical and Schaffer collateral inputs to CA2 pyramidal neurons induced a form of long-term plasticity (input timing-dependent plasticity or ITDP) resulting from a δ -opioid-receptor-mediated long-term depression of feedforward inhibition. We also found that infusion of the δ -opioid receptor antagonist naltrindole into dorsal CA2 impaired social memory. We now write to correct one erroneous experimental result reported in Figure S8, panel A1, and to clarify the nature of a control group used for certain experiments.

In Figure S8A1, we reported that the δ -opioid receptor agonist DPDPE did not alter inhibitory synaptic transmission onto CA3 pyramidal neurons in hippocampal slice experiments. However, after publication of our paper, it was brought to our attention that DPDPE does suppress inhibition in CA3. We have since repeated these experiments using a new batch of DPDPE (Catalog number 1431, Lot 12A, Tocris, Minneapolis) and confirmed that the agonist did, in fact, decrease inhibition in dorsal CA3a. Under voltage clamp, we now find that the inhibitory postsynaptic current (IPSC) in CA3a pyramidal neurons elicited by electrical stimulation in stratum radiatum was reduced to $50\% \pm 10\%$ of its initial baseline level (revised Figure S8A1; $n = 9$, Wilcoxon test, $p = 0.008$), similar to the effect reported in CA2 (Piskorowski and Chevaleyre, 2013). We suspect that the previous aliquot of DPDPE we used may not have been active.

Based on this erroneous result, we argued that the behavioral effects of infusion of naltrindole into dorsal CA2 were unlikely to result from an action of the antagonist in neighboring dorsal CA3 to suppress δ -opioid-receptor-dependent inhibitory plasticity in dorsal CA3. Given that we now agree that inhibitory synaptic transmission in dorsal CA3 is indeed suppressed by δ -opioid receptor activation, we can no longer rule out this possibility. However, as recent findings show that ventral CA3, but not dorsal CA3, is important for social memory (Chiang et al., 2018), we believe that any action of naltrindole in dorsal CA3 is unlikely to account for its behavioral effects on social memory.

The second point concerns a clarification with certain control data. We wish to specify that we used the ITDP data shown in Figure 1E (time plot) and 1F (bar plot at -20 ms) as control data for three experiments performed under identical conditions shown in separate figures (control bar in Figure 2C, E-E pairing in Figure 4D, social novelty occlusion of ITDP in Figures 8E1 and 8E2). In all cases, the control group was treated identically to the experimental group apart from the given experimental manipulation. For the ITDP occlusion experiment, we added two extra cells to the control time plot in Figure 8E1. We had inadvertently omitted these two additional cells in the bar graph plot (Figure 8E2) and now include them in a revised Figure 8. Addition of these two extra data points does not alter our conclusions. We apologize for not specifying the repeated use of a single control group in our paper.



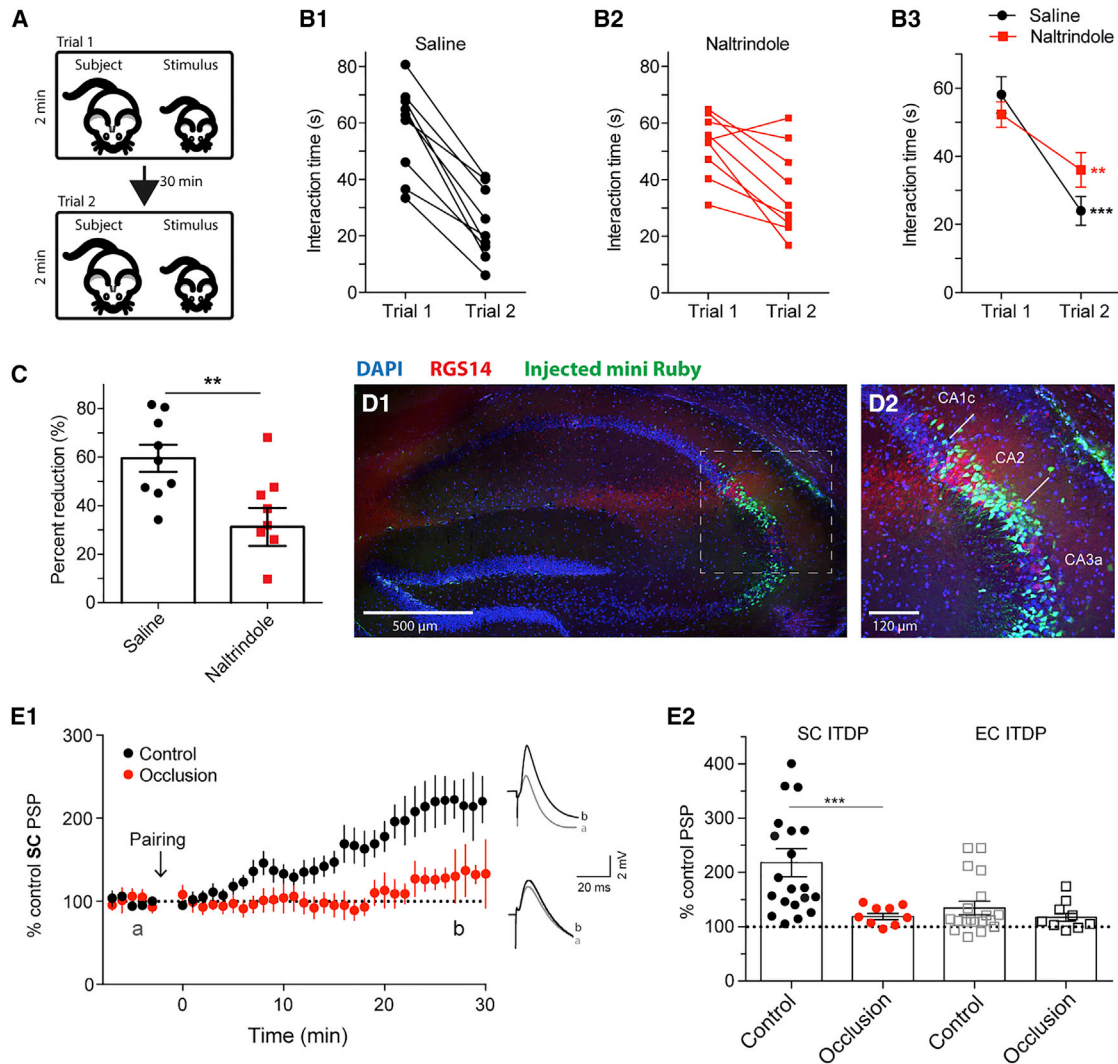


Figure 8. δ -Opioid Receptor Blockade in CA2 Reduces Social Memory and Social Memory Occludes ITDP

(A) Schematic of the direct interaction test for social memory.

(B) Interaction time of saline-injected (B1) and naltrindole-injected (B2) animals in trials 1 and 2 (symbols from individual animals) and superimposed mean \pm SEM (B3).

(C) Percent reduction of interaction time from trial 1 to trial 2. Percent reduction in social interaction was calculated by taking the difference between social exploration time in trials 1 and 2 and then dividing by the social interaction time in trial 1, multiplied by 100%.

(D) Mini-Ruby infusion in the hippocampus and immunohistochemistry for RGS14.

(E) Exposure to social novelty occludes ITDP. (E1) Time course of mean \pm SEM normalized SC-evoked PSP amplitude in CA2 pyramidal neurons obtained in whole-cell current clamp following ITDP induction. Slices were prepared from mice that either experienced a 2 min interaction with a novel juvenile male (social novelty; Occlusion group, $n = 9$ cells) or were continuously housed with littermates (social familiarity; Control group, $n = 15$ cells). Two additional control cells were included in this group compared to that in Figures 1E, 2C, and 4D. Note pronounced reduction in ITDP in response to social novelty ($F = 2.9$, $p < 0.0001$; ANOVA).

(E2) Amplitude of ITDP of PSPs evoked by stimulation of SC (filled circles) or EC (open squares) inputs to CA2 PNs in slices from indicated groups of animals. Symbols show data for single cells; bars show mean \pm SEM. Both SC ITDP and EC ITDP Control groups now include two extra cells. SC ITDP magnitude in Occlusion group ($n = 9$) was significantly less than that in Control group ($n = 21$, $p = 0.0003$; Mann-Whitney test). See also Figure S8.

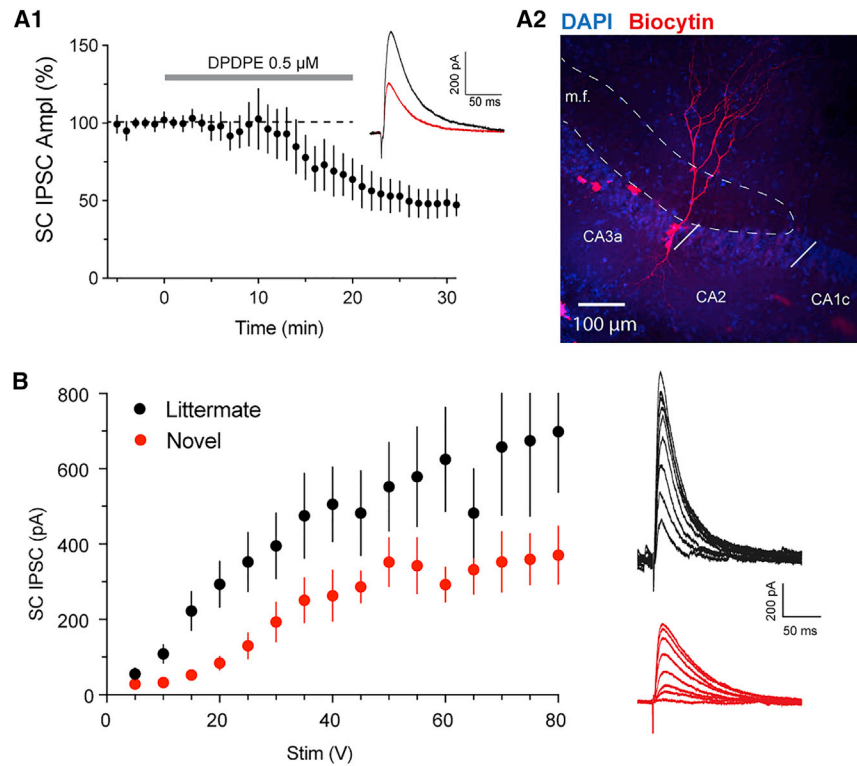


Figure S8.

(A) Panel showing that application of the δ -opioid receptor agonist DPDPE reduced feedforward inhibition in dorsal CA3a pyramidal neurons. (A1) Time course of the IPSC in voltage-clamped CA3a pyramidal neurons (held at -10 mV) induced by SC stimulation during application of 0.5 μ M DPDPE. Insert: example trace of the IPSC before (black) and after (red) DPDPE. Data are represented as mean \pm SEM. (A2) Immunohistochemistry of an acute hippocampal slice stained for biocytin, showing biocytin-filled CA3a pyramidal neuron.

(B) Voltage-clamp recording of IPSCs from dorsal CA2 pyramidal neurons held at -10 mV. The magnitude of feedforward IPSCs recorded in CA2 PNs is plotted against the strength of SC stimulation. IPSC amplitude is reduced in slices obtained from mice that interacted with a novel animal (red; $n = 11$) compared to IPSC amplitude in slices obtained from mice that interacted with a familiar littermate (black; $n = 10$). (Panel B is unchanged.)

REFERENCES

- Chiang, M.C., Huang, A.J.Y., Wintzer, M.E., Ohshima, T., and McHugh, T.J. (2018). A role for CA3 in social recognition memory. *Behav. Brain Res.* 354, 22–30.
- Piskrowski, R.A., and Chevaleyre, V. (2013). Delta-opioid receptors mediate unique plasticity onto parvalbumin-expressing interneurons in area CA2 of the hippocampus. *J. Neurosci.* 33, 14567–14578.